University of Stavanger

Faculty of Science and Technology

MASTER'S THESIS

Study program/ Specialization: Petroleum Engineering	Spring semester, 2011 Open / ~~Restricted access~~
Writer: Terje Tveitdal	…… (Writer's signature)
Faculty supervisor: Dr. E. Kårstad and S.A. Mirhaj External supervisor(s): N/A	
Titel of thesis: Torque & drag analyses of North Sea Wells using new 3D model.	
Credits (ECTS): 30	
Key words: 3-D wellbore friction, Modelling, Realtime, Drilling, Torque and drag, Hydrodynamic viscous force, Contact surface.	Pages: ……74…… Stavanger, …15 June 2011 Date/year

Abstract

Excessive drill string torque and drag is one of the major limitations of extended-reach and horizontal drilling. The torque and drag models are used in the planning phase and during the drilling of a well, as a tool used for monitoring developing hole problems. The models used throughout the industry today are mostly based on equations presented more than two decades ago, little work have been done to improve upon these. The thesis gives a general overview of the various challenges of using such models. It is shown the importance of correcting for friction in the draw works sheaves to get realistic friction factors. A recently published model is used and work has been done to improve this model further. The model has some inaccuracies in the lower part of the string and a new model for drag in the lowest part is proposed. Further is a new criterion presented, for determining whether an element is straight or curved. This new criterion account for radial clearance between drill string and bore hole wall.

Table of Contents

Acknowledgements

I would like to thank S.A. Mirhaj and Dr. E. Kaarstad for guidance and great discussions during the work on the thesis. I would like to thank ConocoPhillips Norway for providing field data. And thanks to Halliburton for providing Landmark's Wellplan software. Finally I would like to thank all my fellow students for all the great times we have had together for the years we have been studying together.

List of tables

List of figures

Nomenclature

A_i =	Pipe inner cross sectional area
A_o =	Pipe outer cross sectional area
BHA =	Bottom Hole Assembly
DD =	Directional Driller
e =	Sheave efficiency
E =	Young's modulus of elasticity
ECD =	Equivalent Circulating Density
ERD =	Extended Reach Drilling
ERW =	Extended Reach Well
d =	Pipe outer diameter
D =	Borehole inner diameter
DL =	Dogleg
DLS =	Dogleg severity
F_1 =	Tension in bottom of a segment
F_2 =	Tension at top of a segment
F_{dl} =	Deadline tension
ID =	Inner Diameter
L =	Length of pipe
MD =	Measured Depth
MWD =	Measurement While Drilling
n =	Number of cables between crown and travelling block
N =	Normal force
OBM =	Oil Based Mud
OD =	Outer Diameter
POOH =	Pull Out Of Hole
P/U =	Pick Up
PV =	Plastic Viscosity
r =	Pipe/connection radius
R =	Radius of a bend
RIH =	Running In Hole
ROP =	Rate of Penetration
RPM =	Revolutions pr. Minute
SPP =	Standpipe pressure
S/O =	Slack Off
t =	Pipe wall thickness
T =	Torque
T&D =	Torque and Drag
TD =	Target Depth
TVD =	True Vertical Depth
V =	Velocity
w =	Buoyed unit pipe weight
W =	Buoyed weight of a segment
W_{tb} =	Weight of the travelling block
WBM =	Water Based Mud
WOB =	Weight On Bit
YP =	Yield Point
α =	Wellbore azimuth

φ = Wellbore Inclination
θ = Absolute change of direction
μ = Coefficient of friction
Ψ = Angle between axial and tangential pipe velocities
ρ = Density

1 Introduction

Excessive drill string torque and drag is one of the major limitations of extended-reach and horizontal drilling. The torque and drag models used throughout the industry today are mostly based on the equations presented by Johancsik in 1984, little work have been done to improve upon these. This thesis presents a field application of a new friction model for petroleum wells. The model is relatively simple and is applicable for any 3 dimensional wellbore trajectory. The friction in the entire well is modelled by two equations, one for straight and one for curved wellbores. Like most friction models it assume that the drill string can be modelled as a soft string like a cable or chain that has no bending stiffness. In the upper part of a well where weight of a string segment is negligible compared to tension load, simplified equations can be used. Friction is modelled in terms of the 3D dogleg. A torque and drag model may incorporate corrections for hydrodynamic viscous drag force, wellbore contact surface, density corrections due to filling of pipe during tripping in and draw works sheave friction.

2 Theory

2.1 Fundamentals of torque and drag

2.1.1 Drag

Drag is the force difference between free rotating weight and the force required to move the pipe up or down in the hole. Pick-up drag force is usually higher than free rotating weight. While slack-off drag force is usually lower than free rotating weight. Drag force is used to overcome the axial friction in the well. This is a phenomena associated deviated wells.

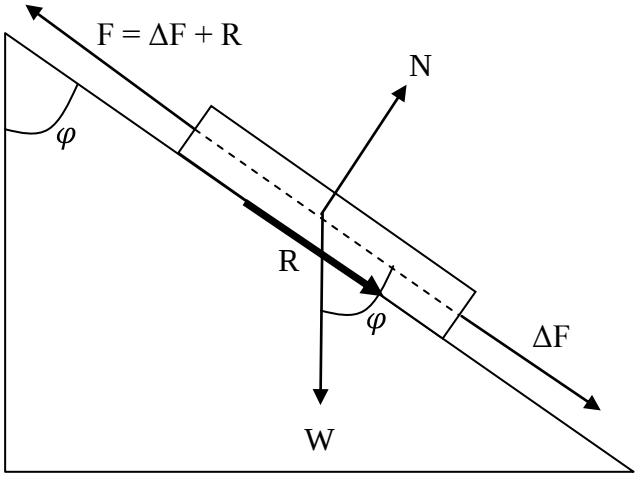

Figure 2.1 Friction in a deviated well

2.1.2 Torque

Torque or moment is generally a force multiplied with a lever arm. When we talk about torque and drilling, then torque is the moment required to rotate the pipe. The moment is used to overcome the rotational friction in the well and on the bit. Torque is lost from the rotating string so that less torque is available at the bit for destroying rock. High drag forces and high torque normally occur together. In a perfect vertical well the torque loss would be zero, except for a small loss due to viscous force from the mud. In a deviated well the torque loss could be great, especially in long complex or extended reach well, where torque loss is a major limiting factor to how long we can drill, as it eventually will overcome the rig or drill strings limitation. Torque is directly proportional to the radius of which rotation occurs and the coefficient of friction and the normal force of which the pipe has against the borehole wall.

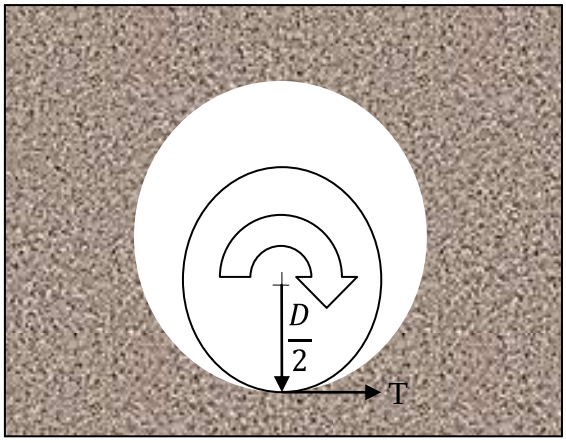

Figure 2.2 Torque to rotate the pipe.

2.2 Which parameters give torque and drag

The true field measured values of torque and drag have always some influence from other contributions. Some of these can be modelled, while other effects are lumped together into the fudge factor which we call a friction factor, which is not the same as the friction coefficient as in pure kinetic sliding friction. The combined effect of all these parameters is what that gives the total torque and drag forces. Broadly we can separate drag forces that are due to hole cleaning or inappropriate mud, and into drag forces associated with the well path.

Hole cleaning and inappropriate mud related drag:

- Mud type, water based mud WBM have less lubricating effect than oil based mud, adding lubricants can reduce torque and drag, although some lubricants may cause formation damage and reduce the well inflow performance.
- Formation properties, different formation lithologies have different lubricating properties due to chemistry and grain size etc. Visualize this by imagining steel rubbing against coarse sandpaper versus rubbing against fine sandpaper, the coarse paper would give the highest friction.
- Hydrodynamic viscous forces
- Fluid density difference during tripping inn due to filling pipe
- Poor hole cleaning, cuttings bed accumulation which is a mechanical wellbore obstruction, could lead to pack-offs, this problem can be reduced by good hydraulics design and proper mud.
- Wellbore instabilities, swelling shale, tight hole, sloughing hole
- Differential sticking, this is caused by the pressure in the well is higher than the pore pressure in the formation, causing the pipe to be pushed into the mud filter cake on the wellbore wall.
- Loss of circulation could give possible loss of lubricity.

Well path related drag:

- Pipe and BHA stiffness. BHA is stiff and stabilizers can interact with formation, which results in higher wellbore friction, especially when BHA is in a high dogleg section.
- Drill string weight, using low weight pipe can be beneficial in a long ERW.
- Stabilizers impact standoff and string stiffness.
- Surface roughness of drill string and casing. Drill pipe connections
- Contact surface
- Doglegs
- Key seating are due to drill string sized channel that are worn into the formation wall in a bend. The wear depends on side force and formation strength. Thus a high dogleg would give high side force and possibly a key seat problem. The problem occurs when larger sized tools such as connections and collars are pulled into the narrower channel and may get stuck. An example of key seating is shown in Figure 2.3.
- Tortuosity, if a well path deviates from a straight line or curve which is assumed by the minimum curvature method, in between two survey points. Then the doglegs vary in between the surveys, this can be due to sliding/rotating while using motor or rotary steerable systems settings changes, WOB fluctuations or over gauge or cavings effects. Short gauge bits have also shown to create holes that are a spiral rather than a straight line. The MWD directional sensor cannot see micro tortuosity from these "micro doglegs", due to the length of the tools they are like a drift in the wellbore. (Gaynor 2002)

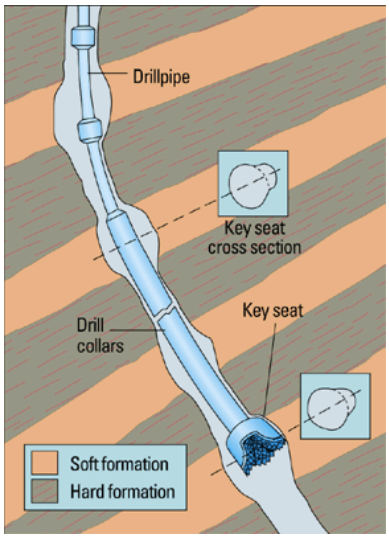

Figure 2.3 Key seating

2.3 Friction

Contact friction as when two relatively smooth solid bodies slide against each other, will be independent of the speed the two bodies slide with, and independent of the contact area. But friction force will be proportional to the contact force of which the surfaces are pushed together with. A friction coefficient, μ relate the ratio of normal force to friction force. The friction coefficient is a dimensionless scalar value. To find the normal force on an incline, trigonometry has to be used. The force needed to drag a block on a plane is shown in Figure 2.4.

$$\mu = \frac{F_f}{F_n} \tag{1}$$

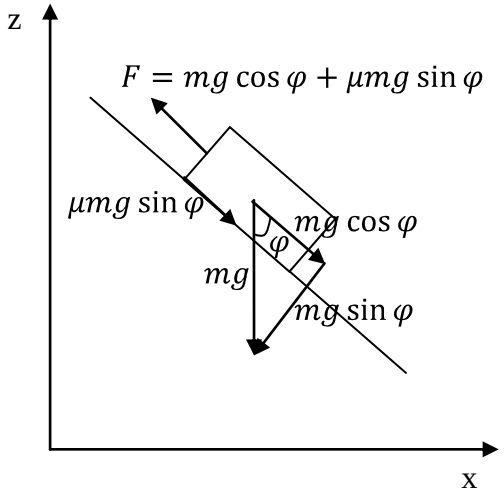

Figure 2.4 Forces on a block sliding on an inclined plane.

The friction coefficient gives friction force as a percentage of the normal force. The direction of friction is always directly opposite the direction of movement.

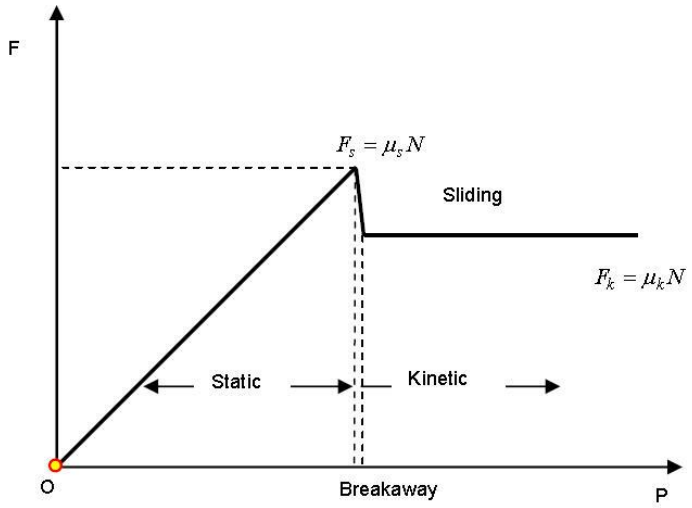

Figure 2.5 Static and dynamic friction.

When the two bodies are at rest we have static friction, which normally is higher than sliding friction. This is shown in Figure 2.5. This is due to interlocking of irregularities of the two surfaces. Static friction will resist motion and counteract any applied force up to a certain maximum where friction is overcome and motion begins. Once the object is in motion, the dynamic friction will resist motion. Coefficients for static and dynamic friction are not equal. Torque and drag models use sliding friction (dynamic friction) effects in their calculations. Currently no torque and drag models account for static friction effects, even though static friction occurs in all wells, but the severity is greatest in extended reach wells. For the first seconds after slips are removed and the string start to move up or down, static friction has to be overcome, and we can define it as static-up drag and static-down drag. For long casing strings in high angle or extended reach wells, the effect can be so severe that casing may fail to reach to planned depth.

Care has to be used when assessing static friction as in a drilling operation, as static friction could be mistaken for differential sticking. Trying to put static friction data into the model would yield unpredictable results due to the complex mechanism of static friction, T & D software should only be used for dynamic friction. In torque and drag software, it is important to know that friction factors are not necessarily interchangeable, as there can be differences in the algorithms used, especially between stiff string and soft string models.

The friction factor is a key parameter in torque and drag modeling because it characterizes the surface to surface interaction which is the heart of model. The friction factor applicable to any situation is a function of many things, including fluid type, composition and lubricity, formation type, casing and tool-joint material and roughness. When significant portions of both cased and open hole exists, it may be necessary to use two or more friction factors, one for the drill string in casing and one for the drill string in formation.

2.4 Extended reach wells ERW

An extended reach well is defined as a well where the ratio between horizontal reach and true vertical depth is larger than 2. In a long ERW, friction forces and torque will be large. Extended reach wells have now been drilled to more than 12 km. Today we are also able to drill complex wells which have a significant changes in azimuth. This gives rise to even large side force and more drag. There are many operational challenges in drilling ERW wells, like torque and drag, drill string and casing design, and hole cleaning. Running completions and casings are often a limiting factor in these wells. This emphasises the importance of having a model that can accurately predict torque and drag forces.

2.5 Buoyancy factor

The weight of a drill string in a well filled with mud is the weight in air minus the weight of mud that the steel in the string displaces, this is also known as the Archimedes principle. For convenience we can define a buoyancy factor as:

$$\beta = 1 - \frac{\rho_{mud}}{\rho_{string}} \tag{2}$$

Buoyancy factor multiplied with weight in air gives the weight of a pipe immersed in mud. If there is a density difference between the fluid in the inside and the outside of the pipe, like during tripping in, during displacing to a different mud weight and cementing. Then the buoyancy factor becomes:

$$\beta = 1 - \frac{\rho_o A_o - \rho_i A_i}{\rho_{string}(A_o - A_i)} \tag{3}$$

Subscript o means outside the pipe and subscript i means inside the pipe. If the fluid density inside and outside the pipe is equal the buoyancy factor equation becomes like (2). A heavy mud will decrease the effective weight of the drill string, and thus decrease side force and the loads from friction and torque. However a heavy mud has more weighing particles which could lead to less lubricity and therefore higher friction.

2.6 Wellbore trajectory

Inclination (φ) is the angle between vertical and the tangent to the wellbore. A vertical well would be zero degree, a horizontal well would be 90 degrees.

Azimuth (α) is the angle between true North and a tangent to the wellbore projected to a horizontal plane. We start from zero which is North, and move clockwise. West is then 270 degrees.

The standard surveying technique of today is to use downhole measurement while drilling MWD directional sensor tools, which measure the direction of the earth gravity by using 3 orthogonally mounted sensitive accelerometers. Hole inclination is found by doing simple trigonometry to measured values. The azimuth direction is measured likewise with 3 orthogonally mounted magnetometers, which measures earth's magnetic field. The measured magnetic direction must be corrected for the magnetic fields declination angle and grid convergence in order to achieve the true north direction. In places like near casings which have significant magnetic interference, gyro tools are used to measure the azimuth direction. The measured depth between two surveys is based on the block position and is updated as the drill pipe joints go down below drill floor (RKB) according to the drillers tally. These 3 measured values, inclination angle, azimuth direction and measured depth between two surveys, are then used to calculate the true vertical depth TVD, and geographic reach in North-South direction and East-West direction. Dogleg DL and dogleg severity DLS which are combination of inclination and azimuth are also calculated.

Dogleg DL is the angle between the tangents of two wellbore positions. A number of methods have been proposed to calculate the wellbore trajectory between the survey points. The exact shape of the wellbore is basically unknown. No method can claim to reproduce the well path exactly, however, after introduction of powerful computers, the "minimum curvature method" has been established as the industry standard. The minimum curvature method assumes that the well path is wrapped on the surface of a sphere between survey points, so that the wellbore has the smoothest possible circular arc. The consensus in industry is that this is the most accurate wellbore trajectory calculation method. The minimum curvature method calculates departure in East, North and Vertical by the following equations:

$$\Delta E = \frac{\Delta L}{2}(\sin\varphi_1 \sin\alpha_1 + \sin\varphi_2 \sin\alpha_2)RF \tag{4}$$

$$\Delta N = \frac{\Delta L}{2}(\sin\varphi_1 \cos\alpha_1 + \sin\varphi_2 \cos\alpha_2)RF \tag{5}$$

$$\Delta V = \frac{\Delta L}{2}(\cos\varphi_1 + \cos\varphi_2)RF \tag{6}$$

where

$$RF = \frac{2}{\theta}\tan\frac{\theta}{2} \tag{7}$$

$$\theta = \cos^{-1}[\sin\varphi_1 \sin\varphi_2 \cos(\alpha_1 - \alpha_2) + \cos\varphi_1 \cos\varphi_2] \tag{8}$$

Index 1 and 2 refer to two consecutive survey stations where 2 is deepest. θ must be in radians. The radius of the sphere of which the well path is wrapped is then found by:

$$R = \frac{\Delta L}{\theta} \tag{9}$$

In order to convert the dogleg from radians to degrees:

$$DL = \frac{180|\theta|}{\pi} \tag{10}$$

The dogleg severity DLS, is found by dividing by the distance between the two positions and it is customary in the industry to multiply this with 30m, in order to get a dogleg pr. 30 meter:

$$DLS = \frac{DL}{\Delta L}30 \tag{11}$$

The dogleg θ depends on both inclination and azimuth, this property is used in the new 3D friction model.

2.7 Cuttings transport

Hole cleaning during drilling of directional wells is a major concern, that should be monitored and controlled. Cuttings accumulations may cause costly problems such as stuck pipe and excessive torque and drag. Cuttings transport in a wellbore depends largely on the inclination, annular flow velocity, viscosity and rotation of the pipe. Generally high rotational speed at above 120 RPM increases hole cleaning, small annuluses have the best effect of rotation. Annular flow velocity and thus flow regime depends on hole size, drill string size and pump rates. Generally hole cleaning increases with annular velocity, up to a certain maximum where the benefit diminishes. Viscosity of the mud is important as a too high viscosity would lead to poor hole cleaning in a horizontal section since the low velocity area would be larger, and pump pressure and ECD would also increase. A too low viscosity would decrease the distance the fluid can carry a particle and reduce the viscous coupling that agitates the cuttings and thereby decreasing the hole cleaning. An increase in rate of penetration ROP increases the hole cleaning requirement. The way cuttings behave in different inclination ranges are as follows (Nazari and Hareland 2010)

In wellbores of 0° to 35°:
Cuttings can move freely around the pipe in a uniform annular velocity. Cuttings are transported by the mud to surface by overcoming the cuttings slip velocity. Slip means that the cuttings move slower to surface than the mud does. When the pumps are shut down cuttings settle downwards. The mud is a shear thinning non-Newtonian fluid which forms a gel when it is at rest. This is to suspend cuttings particles when we are not pumping.

In wellbores of 35° to 50°:
In this range the cuttings form dunes in the low side of the wellbore, because there is a short distance to settle before landing in the low side. Mechanical agitation by rotating the drill string can force the particles into the mud flow again. When pumps are shut down, the dunes might start to avalanche down the hole.

In wellbores of 60° to 90°:
Cuttings particles only have to settle close to the distance of the wellbore diameter to settle on the low side. This creates a continuous cuttings bed on the low side, regardless of flow rate and viscosity. The pipe lie eccentrically on the low side and thus the fluid flow is higher on the top side of the hole than on the lower side, so the fluid flow is above the cuttings, making it almost impossible to clean the well. For cuttings to be transported, agitation by rotation is necessary to send the cuttings up to the high fluid flow area. These high inclinations have higher hydraulic requirement for adequate hole cleaning than lower inclinations.

2.8 Buckling

Axial compression of a pipe will eventually lead to lateral deflection. A drill string in compression will at first go into so-called sinusoidal buckling, where the pipe goes from side to side in a “snaky” manner. If the drill pipe axial compressive load is increased further, the pipe will go into helical buckling, where the drill pipe locks up in a spiralling manner against the sides of the borehole. The onset of buckling will depend of the stiffness of the string components and the outer diameter of components in relation to wellbore and casing. This is important for torque and drag modelling since helical buckling will cause a great increase in the side force between pipe and wellbore walls. Buckling is often seen in small diameter pipe sizes and coiled tubing. Axial loading of pipes is a problem almost unique to the oil industry. Many equations have been derived for calculating the onset of sinusoidal and helical buckling.

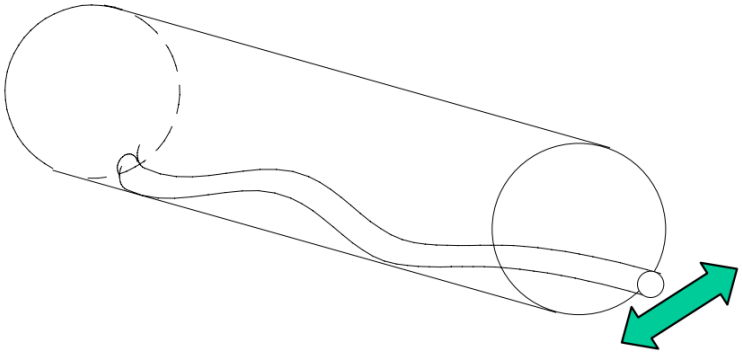

Figure 2.6 Sinusoidal buckling.

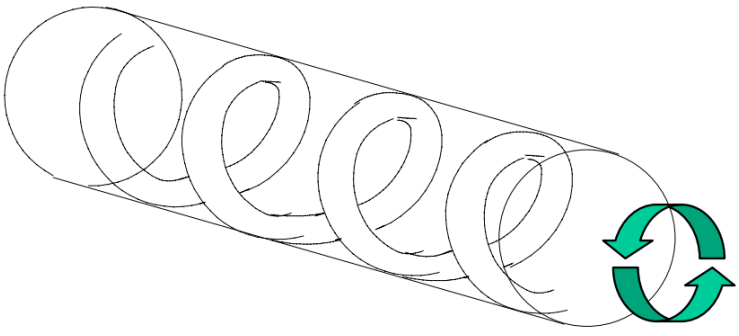

Figure 2.7 Helical buckling.

3 Field data gathering

3.1 Real time data gathering

For the torque and drag models to be usable to assess hole problems. Consistent data from static hookload, up weight, down weight and torque must be collected. Acceptable procedures for measuring these values must be developed and followed. Pick-up, rotating and slack-off should be measured at the same hoisting and lowering speed at all times in order to have good reading consistency. The procedure for collecting data at connections may vary from well to well and with company to company, the most important is that it is done consistently. This procedure making readings before connection has been used successfully by ConocoPhillips:

Pumps are ON for all these measurements:

- Driller drills off weight at Kelly down
- Back ream pulling up at a consistent speed, and according to DD-approved back reaming RPM and DD-approved interval
- interval: 1 single, 2 singles or complete stand of DP
- At the top of DD's back ream interval, stop and rotate freely at 80 RPM for 30 seconds.
- Record the FREE ROTATING WEIGHT and FREE ROTATING TORQUE.
- Then, continue by reaming down at back reaming RPM.
- Pull up at a consistent speed to DD-approved interval without rotary. Make sure we are above stretch distance.
- Record PICKUP WEIGHT.
- Work back down at consistent speed.
- record SLACKOFF WEIGHT.
- Set slips.

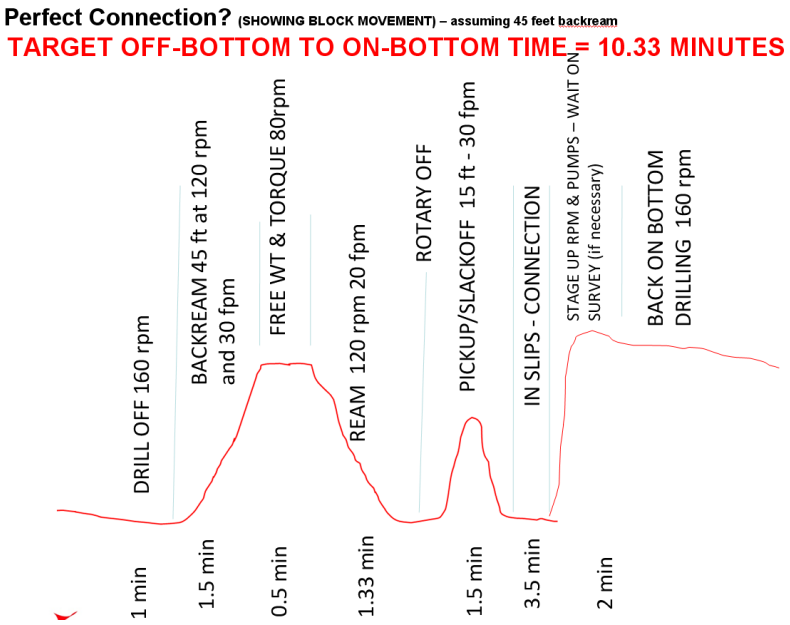

Figure 3.1 Connection procedure.

This procedure should be followed throughout the section and if it is followed, the readings will have good accuracy. Some companies prefer to measure off bottom rotating weight before turning on the pumps after the connection is made. Whether pumps are on or off while measuring free rotating weight makes a small but not insignificant difference due to hydrodynamic viscous drag. An important point is to achieve a good clean baseline before the casing shoe is drilled, then friction factors can be adjusted in for a clean well, this makes it easier to later diagnose drilling problems.

3.2 Automatic gathering of field data

Recently attempts have been made to make the process of collecting data automated. Data processing algorithms collect rig data and recognise rig operations, then these data are updating a torque and drag model automatically. The whole purpose of the system is to monitor the hole condition (Niedermayr et al. 2010) They claim to achieve better consistency by letting computers gather data and thereby removing personal observation, reading errors and interpretation (Cayeux 2009). The torque and drag models was then automated and tracked in real time. The working principle is that hookload and torque is monitored and passed through a filter, then different operations are recognised the measured data are then averaged and fed into the model automatically.

3.3 Measured data

The hookload sensor is a load cell mounted on the deadline in the draw works. A thick cable goes from the cable drum over several sheaves in the crown block in top of the derrick and down to the travelling block sheaves. The deadline goes from the last sheave in top of derrick and down to the load cell and an anchor. A standard draw works is shown in Figure 3.4. A common hookload sensor is shown in Figure 3.2.

Figure 3.2 Example of bolt on hookload sensor.

It is difficult to measure torque directly in a rotary machine. Therefore the torque is commonly measured by top drive electrical current measurement. Measurements are calibrated to not show amperes, but Newton meters or foot lbf by comparing the electric current to motor manufacturer's performance curves, to get a torque reading. An example of such a motor performance curve is shown in Figure 3.3.

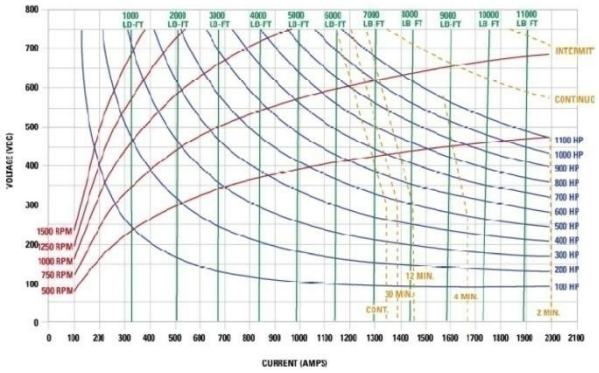

Figure 3.3 Typical motor performance curve, used to convert electric current to torque.

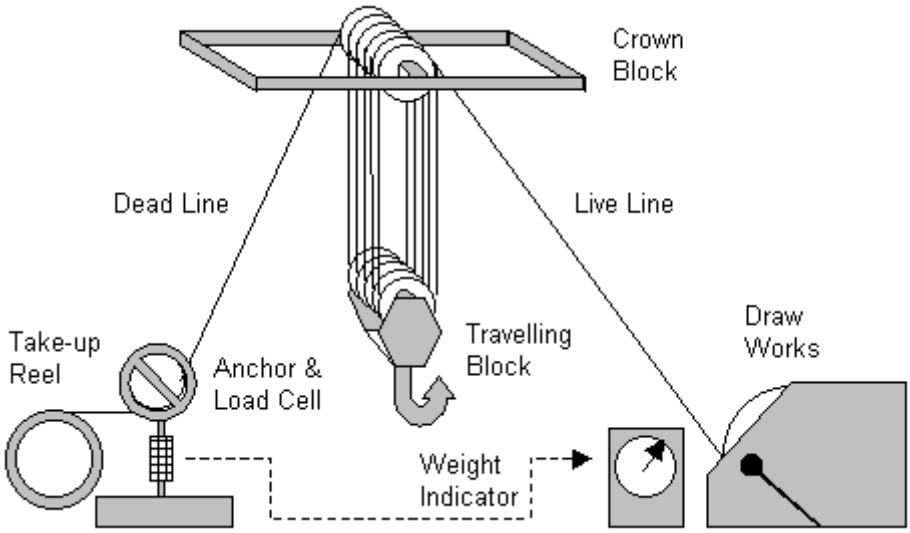

Figure 3.4 Typical draw works rig up.

3.3.1 Sheave friction compensation

The dead line tension F_{dl} is multiplied with the number n of cables between crown block and travelling block, minus the weight of the block and topdrive itself, will give the industry standard way of calculating the hookload.

$$W_{hook} = F_{dl}n - W_{block} \tag{12}$$

If there was no friction in the sheaves, the hookload sensor would give a perfect representation of the weight by multiplying the load cell reading by the number of cables between crown block and travelling block. But since some friction is always present, although small, but not insignificant correction should be made to hookload readings while tripping in or out. True hookload reading depend on sheave efficiency and direction of movement. Typical sheave efficiency is 96-99 %. Due to friction in the sheaves, while tripping out, the fast line will have higher tension than the dead line. In other words, the hookload reading will show too low weight when tripping out, and too high weight while tripping in. The equations were presented by Luke and Juvkam-Wold (1993) for hoisting and lowering. The sheave that the deadline first goes over does not move and can be considered as "inactive" and frictionless sheave, the accurate hookload for tripping can then be calculated by:

$$W_{hoisting} = F_{dl}\frac{e\left(1-\left(\frac{1}{e^n}\right)\right)}{(e-1)} - W_{tb} \tag{13}$$

$$W_{lowering} = F_{dl}\frac{(1-e^n)}{(1-e)} - W_{tb} \tag{14}$$

For a deadline sheave with friction, also called ”active” sheave, then the accurate hookload for tripping can be calculated by:

$$W_{hoisting} = F_{dl}\frac{(1-e^{n})}{(1-e)e^{n}} - W_{tb} \tag{15}$$

$$W_{lowering} = F_{dl}\frac{e(1-e^{n})}{(1-e)} - W_{tb} \tag{16}$$

Experiments done by Luke and Juvkam-Wold (1993) found that the inactive deadline sheave model was the best choice. Of course the weight of the travelling block has to be subtracted from the hookload readings. Another issue with these load cells is calibration. Whenever a load cell is installed or replaced, it should be calibrated. This can be done by placing a calibration sub with a strain gauge on top of a long heavy string, by incrementally increasing the hookload, the load cell readings can be calibrated against the calibration sub readings.

3.4 How do we reduce torque and drag

If a well is drilled and the torque is a lot higher than predicted and exceed the rigs topdrive capacity. A variety of methods are available to reduce torque and drag, the application of such methods can be essential for making sure the TD can be reached before reaching the torque limit of the rig or drill string.

3.4.1 Wellpath

Tortuosity reduction reduces significantly the torque and drag while drilling, the use of RSS are recommended to make the smoothest wellbore. Finding compromises with geologists may be very beneficial, as even small adjustments to the target may reduce the torque (Maehs et al. 2010). Reducing the DLS in build up, drop off and bends can significantly reduce torque and drag especially at the top of the well where tension forces are greatest.

3.4.2 Rotary steerable systems

A hole drilled with a mud motor with a bent sub has generally greater tortuosity than with a RSS, this is due to the steering principle of such tools. Directional drillers obtain the desired DLS by switching from rotary drilling to sliding drilling as many times as needed. Rotary drilling with motor creates smaller hole than sliding. Drilling with motor creates a larger hole than a RSS will do. While sliding, a high DLS is achieved to correct for the direction achieved by rotary drilling, this is a due to a combination of gravity and centralizer placement. This continued alteration is the reason why motors create much more tortuosity than a RSS. Adding a mud motor to an RSS will increase ROP, while RPM at surface can be reduced to minimum and thus reduce the torque. Using RSS with integrated mud motor will reduce surface torque as compared to a conventional RSS (Maehs et al. 2010).

3.4.3 Bit selection

Bit selection is normally based on ROP, steer ability, durability but another factor is important as well. The gauge length can significantly affect the propagation of a cyclic hole. A short gauge bit is more aggressive and creates more calliper variations and what is called micro tortuosity. While a long gauge bit tends to create less calliper variations and a smoother hole (Gaynor 2002). This micro tortuosity is not seen by MWD directional sensors, and will add extra torque and drag. This can be seen as measured torque and drag trends deviate from simulated trends.

3.4.4 Mechanical friction reduction subs

Mechanical friction reducing subs have been tried and proven successful in reducing friction. Use of mechanical friction reduction tools and other techniques for reducing friction have shown to be effective in several deepwater wells in the Gulf of Mexico (Maehs et al. 2010). Various types exist either they consist of mechanical rollers or a sleeve on bearings, which then becomes the effective contact surface. The low friction in a smooth bearing relative to rough steel against rough steel, reduces the torque and drag significantly. The subs are typically placed one pr stand in the sections of the well that sees the highest side force. They have been deployed as a contingency in wells where torque and drag forces became higher than expected, and halted drilling before reaching planned total depth. The use of these mechanical friction reduction subs have reduced torque and drag enough to continue drilling (Long et al. 2009). Although mechanical friction reduction tool have larger OD and are heavier than drill pipe, which would give higher torque and normal force, the effect is outweighed by the reduction of friction that these tools provide. An example of such a tool is shown in Figure 3.5. Another bonus is that casing wear is reduced by these tools.

Figure 3.5 Example of a friction reduction tool.

3.4.5 Mud system

The easiest way to reduce torque and drag is to use oil based mud OBM or synthetic based mud SBM instead of water based mud WBM. It is also possible to add lubricants, even to WBM

3.5 Calibration and interpretation of real time readings

After a model has been made, a typical chart will be generated which shows slack-off, free rotating and pick-up forces for an increasing measured depth. As drilling starts and measured data are plotted on the same chart, the first thing to do is to check the validity of the model, which is done by comparing the measured free rotating weight against the model. Since free rotating weight is independent of friction factors, and is simply the buoyed unit string weight multiplied by the projected vertical depth. Measured free rotating weight should match perfectly with the model. So what is then wrong when they do not match and especially if measured static weight do no longer follow in parallel to the modelled weight and start to follow a different slope.

- Hookload load cell could have wrong calibration.
- Wrong mud weight.
- Wrong weight of drill string components is entered.
- Wrong block weight entered.

Drill string wear and an old worn drill pipe may have lower weight than the specification say it have. BHA weights can also be troublesome as weights are not always accurately given for the myriad of available BHA components. When the model has been tuned or hookload data calibrated, and the free rotating weight looks acceptable, then friction factors can be tuned to match the measured data for pick-up and slack-off. Then the torque and drag model is ready to be used as a tool to monitor hole cleaning or other developing hole problems. As we drill ahead more measured data are plotted. As long as the measured data matches the model, there are no hole problems and hole cleaning is good. If the trend in the measured data starts to diverge from the model it is an indication that a problem is developing. Typically if pick-up weight start to increase and at the same time slack-off start to decrease, it is a good indication that there could be cutting beds accumulation. Since there are many phenomena that can occur during drilling, like differential sticking, tortuosity, key seating, well instabilities like cavings or sloughing shale, it is easy to misinterpret and other relevant data like ECD, standpipe pressure and cuttings on shakers should also be monitored. An increase in ECD is usually a good indicator that cuttings are filling up the wellbore.

3.6 Static hookload

The static hookload or free rotating weight is equal to buoyed unit pipe weight multiplied by projected vertical depth, regardless of inclination (Aadnoy et. al. 1999). In other words a vertical well will have the same static hookload as a deviated well with the same projected vertical depth.
This can be shown for a straight section by:

$$W(\varphi) = w\Delta L \cos\varphi \tag{17}$$

Projected vertical height is:

$$\Delta Z = \Delta L \cos\varphi \tag{18}$$

Combining gives:

$$W(\varphi) = w\Delta Z \tag{19}$$

4 Mathematical modelling

4.1 Torque and drag modelling

Torque and drag modelling software has been used extensively since the 1990's. Especially in complex and long extended reach wells, where the loads are near the limits of equipment material. T & D analysis has been the core of good ERW drilling principle and practice. The models have been important to avoid drilling problems, allowing us to drill further. With longer wells, reservoirs can be drained more efficiently and the number of offshore installations can be reduced, as one installation can drain a larger area. The models are applied in all 3 phases of a well:

In the planning phase torque and drag are two key parameters in the well construction process. Models are used to check if the proposed well path can be drilled and completed with available equipment. Drill string loads are analysed, which then can dictate drill string and equipment size and rig capabilities. The trajectory design can be optimized to minimize torque and drag. Torque must be within safe work limit for the rig and string, allowing for a suitable safety margin. It is also used to check if OBM or WBM should be used. Care has to be taken into account since planned well trajectories are idealized smooth curves, while actual survey data include variable radius of curvature, small doglegs and deviations from planned trajectories. In addition tortuosity in between survey points makes the difference greater. In other words planned well paths are smooth while the real well path is somewhat more crooked. Using planned trajectories will cause the model to predict axial loads and torques that are lower than the actual values. If smooth planned trajectories are used and only friction factor is increased to correct for hole irregularities, it would have the limitation that it would predict zero torque and drag in the vertical part of a well, because side forces are zero in vertical sections. Therefore actual survey data should rather be used or some tortuosity, rippling or crookedness could be applied to the planned trajectories. Many different algorithms for superimposing this rippling have been suggested, including sine wave and random alteration of azimuth and inclination by various magnitudes of amplitude and wavelength.

Challenging and complex wells are often modelled in real-time, the benefit is that drilling problems can be detected at an early stage, allowing us to take action and mitigate the smaller problems before it escalade into a big problem that could give serious well damage. The hookload is then measured in real time at connections and pick-up weight, slack-off weight and free rotating off bottom weight and torque is recorded and compared to calculated values. If recorded values match the model, it indicates that the well has good hole cleaning. When recorded values deviate from the model, it's a good indicator that there is a problem downhole. The problem might be due to key seating, differential sticking, cuttings bed accumulation. Whatever the problem is other factors like ECD, standpipe pressure, pit volume must be checked to evaluate what the problem is. In order to obtain best results, real time surveys should update the model in order to include deviations from planned well trajectory and directional drilling errors. Torque and drag models are the best tool we have for monitoring hole conditions. In real-time it is also possible to back-calculate friction factor from measured hookload by iterating until a match between measured value and the model (Lesage 1988) is found. A plot of calculated friction factors versus

depth is then used to identify downhole problems. This can also be calculated in drilling mode if downhole weight on bit and downhole torque on bit is available. Torque and drag models are steady state models, which means the calculations are only made for string movement in a steady manner, sudden transient effects are not incorporated.

In post drilling a detailed analysis can be an aid in revealing the true cause of problems, which previously was unexplainable. The post drilling analysis allows us to make changes to operational procedures, so we can avoid problems for the next well. The measured data can be used to give us better understanding and allow us to plan the next well better. Post analysis may also lead to a more accurate friction factor, by including local information such as formation lithology, permeability and mud properties. The gained information can be used to evaluate better well trajectories and kick-off points depths, and correcting casing setting depths, in order to avoid hole problems being encountered in the evaluated wells.

To summarize, a torque and drag model has the following use:

- Trajectory design to minimize torque and drag forces.
- Determining hole condition to determine if problems are arising.
- Drill string design to reduce torque and drag.
- Monitoring hole cleaning in real time.
- Monitoring friction when running casing.
- Determine the onset of drill pipe buckling.
- Determine the possibility of reciprocating casing during cementing.
- Providing lateral load inputs for casing wear models.
- An aid in determining if a changes to the mud is necessary.
- Calculating WOB in highly inclined wells with high frictional drag.
- Determining if drill string torque limits may be exceeded.
- Aid in making strategic decisions on mud systems.

4.2 The standard model

Torque and drag modelling began with Johancsik et al. (1984). They presented a simple and user friendly model. Johancsik assumed that torque and drag was entirely caused by sliding friction. He used the standard Coulomb friction model and set up a force balance for a pipe element in order to find the normal force between pipe segment and borehole wall. He assumed that the normal force was caused entirely by tension against the curvature and the weight of the segment. He decomposed the normal force and assumed that the total normal force of a segment would be the vector sum of the horizontal and vertical components. The model considers the string to be made up of short segments joined by connections which transmit tension and torsion. The equation for friction is applied to each segment, with the calculations starting at the bottom of the drill string and proceeding upward to the surface. Each short element contributes to small increments of torque, axial drag and weight. These forces and torques are summed to produce the total loads on the string. This model is thought to be an approximation of real drill string behavior.

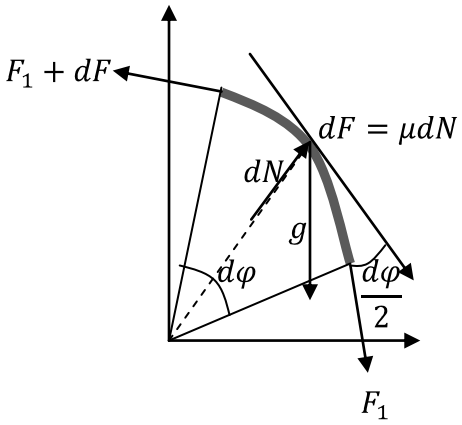

Figure 4.1 Forces on an infinitesimal segment.

By investigating Figure 4.1 we see that the normal force when using polar coordinates is:

$$dN_v = (F_1 + dF)\, sin\left(\frac{d\varphi}{2}\right) + F_1 \sin\left(\frac{d\varphi}{2}\right) + w\, R \sin\varphi\, d\varphi \tag{20}$$

For small angles (in radians):

$$\sin\left(\frac{\varphi}{2}\right) \approx \left(\frac{\varphi}{2}\right)$$

We get:

$$dN_v = 2F_1\left(\frac{d\varphi}{2}\right) + dF\left(\frac{d\varphi}{2}\right) + wR\sin\varphi\, d\varphi$$

And since: $dF_1\frac{d\varphi}{2} \approx 0$

We then have normal force contribution in vertical direction:

$$dN_v = F_1 d\varphi + wR\sin\varphi\, d\varphi \tag{21}$$

In horizontal direction we have a normal force of:

$$dN_h = (F_1 + dF)\,sin\left(\frac{d\alpha}{2}\right)\sin\varphi + F_1\sin\left(\frac{d\alpha}{2}\right)\sin\varphi$$

This then reduces to:

$$dN_h = F_1 d\alpha\sin\varphi \tag{22}$$

In tangent direction we have:

$$(F_1 + dF)\cos\left(\frac{d\alpha}{2}\right) - F_1\cos\left(\frac{d\alpha}{2}\right) \pm \mu|dN_t| = 0 \tag{23}$$

For small angles (in radians):

$$\cos\left(\frac{d\alpha}{2}\right) \approx 1$$

We then reduce to the incremental friction force which is product of the normal force and friction factor:

$$dF = \pm\mu|dN_t| \tag{24}$$

The normal force N_t is the vector sum of the horizontal and the vertical normal force so:

$$dF = \pm\mu((F_1 d\alpha\sin\varphi)^2 + (F_1 d\varphi + wR\sin\varphi\, d\varphi)^2)^{\frac{1}{2}} \tag{25}$$

Letting the approximation that $d \approx \Delta$ and since:

$$wRd\varphi = W \tag{26}$$

Adding a term for the projected weight, Johancsik ended up with an equation for the drag of a segment:

$$F_2 = F_1 + W\cos\varphi \pm \mu((F_1\Delta\alpha\sin\varphi)^2 + (F_1\Delta\varphi + W\sin\varphi)^2)^{\frac{1}{2}} \tag{27}$$

F_1 is the force on bottom of the segment. Where + means hoisting and – means lowering.

In a straight section without any curvature $\Delta\varphi = \Delta\alpha = 0$
And the equation reduces to:

$$F_2 = W\cos\varphi \pm \mu W \sin\Phi \tag{28}$$

In a horizontal bend section, the equation would reduce to:

$$F_2 = F_1 \pm \mu((F_1\Delta\alpha)^2 + (W)^2)^{\frac{1}{2}} \tag{29}$$

A vertical bend would be:

$$F_2 = F_1 + W\cos\varphi \pm \mu(F_1\Delta\varphi + W\sin\varphi) \tag{30}$$

He assumed that the side forces in a bend due to the stiffness in pipe could be considered negligible, so the string is modelled as a cable, chain or rope with no stiffness. Therefore the string is therefore called a soft-string model where bending moments are not considered. Later Sheppard et al. (1987) changed the model to standard differential form, and included mud pressure effect. This model is widely available and has been used throughout the industry. If there is something as a standard model this is the one. Numerous companies offered torque and drag software, but almost all are based on the same equations, if the inputs are the same, they would all yield similar results (Mason and Chen 2007). A major assumption is that the string is in continuous contact with the wellbore over the entire length, thus radial clearance is ignored. It could therefore ignore the direction of normal force vectors and only consider their magnitude.

There is question about how good is the standard model is. The consensus in the industry with a lot of field experience is that it is generally pretty good, although not perfect. And sometimes it performs poorly. If the segment length was infinitesimal small, the model would be exact. Longer elements introduce errors due to neglecting second order terms (Johancsik 1984). The error is small when the curvature of the segment is small. The standard model has shown to perform poorly on short radius wells and on complex 3D wells (Mitchell 2009).

In theory the friction factors for torque hoisting and lowering should all be the same. Often the friction coefficients that are needed to match real drag data are different than friction factors needed to match torque data, sometimes even different friction factors for lowering and hoisting are needed (Mitchell 2009). The friction factors may even change from trip to trip. That is unphysical and is a good indication that something is wrong with the model. Fudging by using several friction factors to match measured data is a convenience, but a strong indicator that the model could be improved.

4.3 The new 3D friction model

4.3.1 Introduction

The old standard model and the new model have many similarities. Both models assume linear Coulomb friction and assume that friction between pipe and borehole wall is equal to normal force multiplied with a friction factor. In a straight section there is no difference, the equations used are identical. In any curved section the models only differ in the way side force is calculated**.** Aadnoy and Andersen (2001) derived exact analytical equations for torque and drag in drop-off, build-up and side-bend geometries. Later Aadnoy and Djurhuus (2008) found that the solutions had a lot of symmetry, which led to further simplifications of the equations. They also showed that the same equations could handle pipe in compression through a bend. These simplified equations were limited to drop-off and build-up segments in vertical plane. Recently Aadnoy, Fazaelizadeh and Hareland (2009) published a fully analytic 3-dimensional torque and drag model which is based on the absolute angle change, or dogleg severity. The model also had capability of combined axial and tangential motion, such as for reaming and drilling. A whole well can then be analysed by two sets of equations, one for straight sections and one for curved sections.

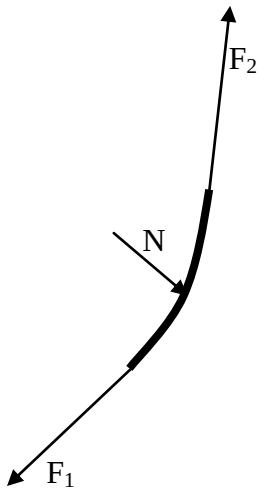

Figure 4.2 New 3D model.

The model describes the hookload while hoisting, static and lowering, and reaming and back reaming. Two equations describe torque and drag for a straight section. Two other equations describe the torque and drag for a curved segment. The length of one segment, in the planning phase, can be a full build-up, drop-off or tangent section. While for real drilling data, one segment is usually the measured distance of wellbore between two surveys. The model starts from the bottom of the well and calculates tension force increment and torque increment for every segment. The tension force on top of one segment is used as the tension in the bottom of the next segment higher up, this continues to the top of the well.

4.3.2 Assumptions

Like the Johancsik model, the new model assumes the drill string is made up of short segments joined by connections which transmit tension, compression and torsion. All soft-string algorithms ignore the bending stiffness of drill pipe and collars in the BHA, and the effect of stabilizers interaction with formation. These algorithms will result in a slight under-estimation of the amount of drag and torque in the stiff BHA section, especially if the hole is crooked with high doglegs. In the drill string section the effect of bending stiffness is minimal and can be ignored. To compensate for bending stiffness in the BHA an over-estimation of the friction factor can be done. The soft-string algorithms also ignore radial clearance between string and borehole. The strings path is assumed to be exactly the same as the hole path. The string is therefore assumed to have constant contact with the wellbore throughout the well.

4.4 Inputs to the model

- Drill string description including: ODs, IDs, weights and lengths
- Actual survey data to MD, including: MD, azimuth and inclination.
- Planned survey data to TD, i including: MD, azimuth and inclination.
- Friction factors in cased hole and open hole.
- Mud properties: density, plastic viscosity and yield point.
- Travelling block weight
- Casing depths and weights
- Pump rate, for hydraulics calculations
- Torque On Bit, (if a TOB sub is in the BHA)
- Weight On Bit, (if a WOB sub is in the BHA)
- RPM
- Bit depth
- Hookload
- Torque at surface

4.5 Friction factors

Torque and drag equations use normal force and a friction factor to calculate the drag forces and torque. If the friction factor is unknown it can be adjusted by iteration to match simulated results with field measured data. Any simulated result is inaccurate due to complexity and multitude of variables that affect the friction factor. In order for the model to have any practical value and obtain realistic results, it is essential to remove as much "fudge" as possible from the "lumped" parameter which is called a friction factor. We therefore can apply corrections for various effects, such as contact surface, hydrodynamic viscous drag, temperature and sheave friction.

4.6 End conditions

The boundary conditions at the end of the string will depend on the operation being simulated. At the end of the string then $F_1 = 0$ when the bit is rotated off bottom or when tripping in or out. For simulating drilling, when the bit is on bottom, a positive value is given to F_1, to simulate the Weight On Bit WOB. Likewise for simulating the Torque On Bit, TOB, a positive value is given to T_1.

4.7 Derivation of the new 3D model equations

4.7.1 Drag in straight inclined section without rotation

In a straight section of a wellbore, the friction will be independent of tension in the string. The only contributing factor to side force is the weight of the string. The force on top of a straight section is then:

$$F_2 = F_1 + w\Delta L(\cos\varphi \pm \mu \sin\varphi) \tag{31}$$

F_1 is the force on bottom of the segment. Where + means hoisting and – means lowering. The forces on a straight section are exactly similar to the forces on a block sliding on a plane, as shown in Figure 2.4. This equation for drag in a straight section is identical to the model proposed by Johancsik. In a straight section there is no change in inclination and azimuth, so $\Delta\varphi = 0$ and $\Delta\alpha = 0$. The Johancsik model for drag is:

$$F_2 = F_1 + W\cos\varphi \pm \mu\sqrt{(F_1\Delta\alpha\sin\varphi)^2 + (F_1\Delta\varphi + W\sin\varphi)^2} \tag{32}$$

This will for a straight section reduce to:

$$F_2 = F_1 + W\cos\varphi \pm \mu\sqrt{(W\sin\varphi)^2} \tag{33}$$

Reducing and inserting: $W = w\Delta L$, we get:

$$F_2 = F_1 + w\Delta L(\cos\varphi \pm \mu\sin\varphi) \tag{34}$$

The result (31) is identical to (34), so it has been shown that the new model and Johancsik model are identical for straight sections.

4.7.2 Torque in straight incline section without rotation

Torque is the normal weight component multiplied with a coefficient of friction and the radius of the pipe. For drill pipe that would be the tool joint radius, for collars it would be the OD, and for BHA it would be the centralizer OD.

$$T_2 = T_1 + \mu r w\Delta L\sin\varphi \tag{35}$$

4.7.3 Drag in a curved section without rotation

In a curved section the side force between string and wellbore depends on the tension and the side force due to the weight of the string. Near the top of a well the tension causes a lot larger side force than the weight of the string in the section. We can therefore assume the string as weightless and if we look at a curved segment in Figure 4.3, we get the infinitesimal normal force:

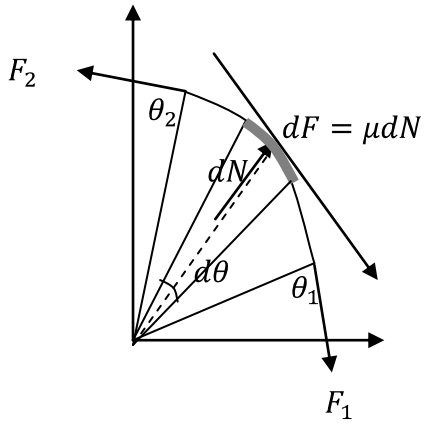

Figure 4.3 Forces on a curved segment.

$$dN = Fd\theta \tag{36}$$

This leads directly to the friction force:

$$dF = \mu Fd\theta \tag{37}$$

We get an integral

$$\int_{F_1}^{F_2} \frac{dF}{F} = \int_{\theta_1}^{\theta_2} \mu d\theta \tag{38}$$

Integration between θ_1 and θ_2 gives:

$$F_2 = F_1 e^{\pm\mu|\theta_2-\theta_1|} \tag{39}$$

We then add a term for the weight of the string, which is buoyed unit weight of pipe multiplied by projected vertical height.

$$F_2 = F_1 e^{\pm\mu|\theta_2-\theta_1|} + w\Delta TVD \tag{40}$$

Projected vertical height may be found by several methods, for instance with the radius of curvature method, it will be:

$$\Delta TVD = \Delta L\left(\frac{\sin\varphi_2 - \sin\varphi_2}{\varphi_2 - \varphi_1}\right) \tag{41}$$

4.7.4 Torque in a curved section without rotation

When tensile force is so large that we can ignore the side force due to the weight of the pipe, then we find the torque by multiplying side force with radius and friction factor:

$$T = T_1 + \mu r F_1 |\theta| \tag{42}$$

4.7.5 Combined motion

The angle between axial and tangential velocity is:

$$\Psi = \tan^{-1}\left(\frac{V_a}{V_t}\right) = \tan^{-1}\left(\frac{V_a\ 60}{2\pi RPM}\right) \tag{43}$$

If Ψ = 0º then there is rotation only.
If Ψ = 90º then there is axial motion (up/down) only.

Straight section

$$F_2 = F_1 + w\Delta L\cos\varphi - \mu w\Delta L\sin\varphi\sin\Psi \tag{44}$$

$$T_2 = T_1 + \mu r w\Delta L\sin\varphi\cos\Psi \tag{45}$$

Curved section

$$F_2 = F_1 + F_1\left(e^{\pm\mu(\theta_2-\theta_1)} - 1\right)\sin\Psi + w\Delta TVD \tag{46}$$

$$T_2 = T_1 + \mu r F_1 |\theta|\cos\Psi \tag{47}$$

4.8 Stiff string models

Various attempts have been done to create a friction model that account for the string bending stiffness (flexural rigidity) and radial clearance, such models are called stiff-string models. There are currently no "industry standard" formulation for stiff string models. Due to the stiffness of a string, such models should give higher side force in a bend, and probably lower side force at the end of the bend where the pipe straightens. A stiff string model could in theory be beneficial when the trajectory is highly tortuous with high doglegs and there is a stiff BHA or casing. The stiff string models

were developed to overcome soft string models limitations where they under predict the drag especially for the BHA, however field experiences indicate that stiff string models fail to accurately model effects of radial clearance (Mason 2007). More studies should be performed to determine when stiff string models should be applied. Stiff string models are not used in this thesis, and are not discussed further.

4.9 Contact surface effect

A pipe dragged along a flat surface will have less friction than the same pipe being dragged through a wellbore (Maidla and Wojtanowicz 1987). An approximated correction factor which is based on hole size and pipe diameter for every string element, can be applied to the friction factor. They showed that when a cylinder with outer diameter d moves through a pipe with a slightly larger inner diameter D, then the friction force will be $\frac{4}{\pi}$ greater than if the pipe was dragged along a flat surface.

$$F_d = \frac{4}{\pi}\mu N \tag{48}$$

A pipe in a well has generally a smaller OD than the ID of the wellbore and a correction factor C_s will apply, this will be somewhat smaller than $\frac{4}{\pi}$:

$$F_d = C_s \mu N \tag{49}$$

The correction factor varies between 1 and $\frac{4}{\pi}$, dependent on the contact surface angle γ_i of the section, γ_i varies between 0 and 90 degrees.

$$C_{si} = \frac{2}{\pi}\gamma_i\left(\frac{4}{\pi} - 1\right) + 1 \tag{50}$$

Where contact surface angle is given by:

$$\gamma_i = \left|\tan^{-1}\frac{2X_i}{2Y_i - D_i + d_i}\right| \tag{51}$$

Where:

$$Y_i = \frac{1}{4}\left|\frac{D_i^2 - d_i^2 + (D_i - d_i + 2\Delta d_i)^2}{(D_i - d_i + 2\Delta d_i)}\right| \tag{52}$$

$$X_i = \frac{1}{2}\left|d_i^2 - 4Y_i^2\right|^{\frac{1}{2}} \tag{53}$$

$$\Delta d_i = \frac{\pi}{24E_i} N_i \frac{d_i}{t_i} \tag{54}$$

Since Young's modulus E for steel is very high, Δd will be very small and can be ignored. Then we get a friction factor correction that only depends on the string outer diameter and wellbore diameter. It can be reduced to:

$$C_s = \frac{2}{\pi}\tan^{-1}\left(\frac{(D_i - d_i^2)^{1/2}}{d_i}\right)\left(\frac{4}{\pi} - 1\right) + 1 \tag{55}$$

We then get a contact surface corrected friction factor by:

$$\mu_{corrected,i} = \mu_i\left(\frac{2}{\pi}\tan^{-1}\left(\frac{(D_i - d_i^2)^{1/2}}{d_i}\right)\left(\frac{4}{\pi} - 1\right) + 1\right) \tag{56}$$

The effect of contact surface mentioned here is very easy to apply as it only depends on borehole size and string diameter, however, as shown by Fazaelizadeh (2010) the effect is small and is therefore not investigated further in this thesis.

4.1 Hydrodynamic viscous force and circulation of mud

Circulation of mud causes an apparent reduction of the weight of the string. This effect is dependent of hole size, drill string size and mud rheology and pump rate. Smaller hole sizes seem to be most affected. In a borehole where we have a string where we pump down mud, we have liquid flow that is at least partly turbulent. Friction from viscous drag is not linear, and various complex equations have been used.

4.2 Hydrodynamic viscous drag force and axial motion

The pressure gradient in annulus depends on annular flow velocity, mud properties, flow regime, pipe velocity. Some torque and drag models does not take into account effects of fluid flow, attempting to simulate weight with pump on with a non-fluid flow enables model could give erroneous results. The biggest problem is the great number of rheological models available, so the calculated results have a great variability. The frictional losses depends on annular velocity and hydraulic diameter and viscosity. The accuracy of all these may be debated. The viscosity of non Newtonian drilling fluids is such that shear stress versus shear rate is not linear. So the viscosity is not uniform over a cross sectional area, viscosity may also be dependent of temperature. The Reynolds number depends on viscosity, flow velocity and diameter. In other words, a calibration of several parameters may be necessary to accurately model such a highly complex problem. Surge and swab calculations can be used to calculate pressures associated with axial pipe movement (Maidla 1987). The calculation procedure is based on the theory for viscous drag for Power law and Bingham plastic fluids in a borehole. Calculation of mud clinging constant for laminar flow:

$$C_c = \frac{\delta^2 - 2\delta^2\ln(\delta - 1)}{2(1 - \delta^2)\ln\delta} \tag{57}$$

Mud clinging constant for turbulent flow:

$$C_c = \frac{\sqrt{\frac{\delta^4 + \delta}{1 + \delta}} - \delta^2}{1 - \delta^2} \tag{58}$$

Where δ is the ratio of pipe diameter and borehole diameter. The average effective annular velocity which produces the viscous drag component of surge pressure is:

$$v_{ae} = v_{pipe}\left(\frac{\delta^2}{1 - \delta^2} + C_c\right) \tag{59}$$

The Reynolds number N_{Re} can then be found for annular flow, assuming a Bingham-plastic drilling fluid:

$$N_{Re} = 926.4 \cdot \frac{\rho v_{ae}(D - d)}{PV} \tag{60}$$

Where laminar flow: $N_{Re} \leq 2100$
And turbulent flow: $N_{Re} > 2100$
And the Reynolds number N_{Re} can be found for annular flow, assuming a Power-law fluid:

$$N_{Re} = 10.9 \cdot 10^4 \cdot \frac{\rho v_{ae}^{2-n}}{PV}\left(\frac{D - d}{48} \cdot \frac{n}{2n + 1}\right)^n \tag{61}$$

Where laminar flow: $N_{Re} \leq 3479 - 1370 \cdot n$
And turbulent flow: $N_{Re} > 4270 - 1370 \cdot n$

Calculation of friction factors: for Reynolds numbers less than 10^5, a Straight line approximation of the Colebrook function for Bingham plastic fluid yields an accurate friction factor, we then have a Fanning friction factor. Power-law fluids may also use Fanning friction factors for low Reynolds numbers with acceptable errors. Fanning friction factors are found for laminar and turbulent flow by:

$$f_{lam} = \frac{16}{N_{Re}} \tag{62}$$

$$f_{turb} = \frac{0.0791}{N_{Re}^{0.25}} \tag{63}$$

Viscous pressure gradient is then found by Bingham plastic model by:

$$\frac{\Delta P}{\Delta L} = \frac{f v_{ae}^2 \rho}{25.78(D - d)} \tag{64}$$

Viscous pressure gradient is found for laminar and turbulent flow by Power law model by:

$$\frac{\Delta P_{lam}}{\Delta L} = \frac{k}{14.4 \cdot 10^4 (D-d)} \left(\frac{48}{D-d} \cdot \frac{2n+1}{n} \right)^n \tag{65}$$

$$\frac{\Delta P_{turb}}{\Delta L} = \frac{f v_{ae}^2 \rho}{21.1(D-d)} \tag{66}$$

Finally the hydrodynamic viscous force can be calculated for each segment:

$$F_{Di} = \frac{\pi}{4} \left(\frac{\Delta P}{\Delta L} \right)_i \Delta L_i d_i^2 \tag{67}$$

The effect of hydrodynamic viscous drag and axial motion is mentioned here because it gives a small effect. But it is out of the scope of this thesis to pursue this complex problem any further.

4.3 RPM dependence of torque

Field experiences have shown that torque is dependent on RPM. Viscous drag contribute somewhat, but the effect is relatively small. It is probable that at certain rotational speeds the string gets excited, an increase in torque is then seen due to whirl, vibration and gyroscopic precession. These are transient dynamic effects that are not currently implemented in any torque and drag models. Therefore it is important that in order to achieve consistency, torque readings should be done at the same RPM throughout a section.

4.4 Potential pitfalls in modelling

- A torque and drag model cannot be used to see if a casing will go through a sharp dogleg. Due to the nature of a soft string model, radial clearance is ignored, so even if a simulation looks good, the casing might be impossible to get through the dogleg.
- Friction factors from drilling runs should not be used directly for casing runs. Different factors may apply, even though the metal to metal and metal to formation friction would be the same. This is due to the nature of the friction factor which is more like a correlation factor which lumps together several effects such as tortuosity, bending stiffness, hydrodynamic viscous drag and contact surface difference due to the increased size of casing relative to drill string size.
- Static friction is very complex and unpredictable, using static friction in a torque and drag model is inappropriate. A torque and drag model is usable for modelling with dynamic friction (Mason 2007).
- Torque is also dependent on RPM, due to dynamic or transient effects which are not yet incorporated into the models. Therefore, torque readings should be made at a consistent RPM throughout a section.

4.1 A different approach to drag

Johannes Djurhuus defined the problem of drag in a bend in the vertical plane slightly different from Aadnoy and Andersen (2001). He came up with a model for drag in a bend which possessed a lot of symmetry. Note that his solution is only applicable to a vertical bend, in other words only 2D, not for a 3D bend with changes in azimuth. The exact solution for drag in a vertical bend from Aadnoy and Djurhuus (2008):

$$F_2 = F_1 e^{AB\mu(\varphi_2-\varphi)} + \frac{wR}{1+\mu^2}\left[A(1-\mu^2)\left(\sin\varphi_2 - e^{AB\mu(\varphi_2-\varphi_1)}\sin\varphi_1\right) - 2B\mu\left(\cos\varphi_2 - e^{AB\mu(\varphi_2-\varphi)}\cos\varphi_1\right)\right] \quad (68)$$

The sign of A and B are shown in table 4.1 for different operations and geometries.

Sign Constant	Buildup hoisting	Dropoff hoisting	Buildup lowering	Dropoff lowering
A-tension	+	+	−	−
A-compression	−	−	+	+
B	−	−	−	+

Table 4.1 Sign of A and B for different geometry.

4.2 Summary of equations

4.2.1 Summary of equations from Johancsik

Hoisting and lowering, straight	$F_2 = F_1 + W\cos\varphi + \mu W\sin\varphi$
Hoisting and lowering, 3D	$F_2 = F_1 + W\cos\varphi \pm \mu\sqrt{(F_1\Delta\alpha\sin\varphi)^2 + (F_1\Delta\varphi + W\sin\varphi)^2}$
Vertical bend	$F_2 = F_1 + W\cos\varphi \pm \mu(F_1\Delta\varphi + W\sin\varphi)$
Horisontal side bend	$F_2 = F_1 \pm \mu F_1\Delta\alpha$

Table 4.2 Summary of the "standard" model

4.2.2 Summary of drag equations from Djurhuus

Hoisting and lowering	$F_2 = F_1 e^{\pm\mu(\varphi_2-\varphi_1)} + \frac{wR}{1+\mu^2}((1-\mu^2)(\sin\varphi_2 - e^{\pm\mu(\varphi_2-\varphi_1)}\sin\varphi_1) - 2(\pm\mu)(\cos\varphi_2 - e^{\pm\mu(\varphi_2-\varphi_1)}\cos\varphi_1))$
Torque static	$T_2 = T_1 + \lvert r\mu\{F_1(\varphi_2-\varphi_1) + wR[2(\cos\varphi_1 - \cos\varphi_2) - (\varphi_2-\varphi_1)\sin\varphi]\}\rvert$

Table 4.3 Djurhuus's equations for vertical bends

		String in compression		String in tension	
		φ	μ	φ	μ
Build up bend:	Hoisting	+	−	−	−
	Lowering	−	−	−	+
Drop-off bend:	Hoisting	+	+	−	+
	Lowering	−	+	+	+

Table 4.4 Sign convention in Djurhuus' drag equations

4.2.3 Summary of straight section equations

Static weight	$F_2 = F_1 + w\Delta L \cos\varphi$
Hoisting force	$F_2 = F_1 + w\Delta L(\cos\varphi + \mu \sin\varphi)$
Lowering force	$F_2 = F_1 + w\Delta L(\cos\varphi - \mu \sin\varphi)$
Torque	$T_2 = T_1 + \mu r w \Delta L \sin\varphi$

Table 4.5 Summary of straight section equations

4.2.4 Static weight of a bend segment

Drop-off static weight	$F_2 = F_1 + w\Delta TVD$
Build-up static weight	$F_2 = F_1 + w\Delta TVD$
Side bend static weight	0

Table 4.6 Static weight of a bend

Where true vertical depth of a segment may be found with minimum curvature method, or by approximation by:

$$\Delta TVD = R(\sin\varphi_2 - \sin\varphi_1)$$

Or alternatively, with radius of curvature method:

$$\Delta TVD = \Delta L\left(\frac{\sin\varphi_2 - \sin\varphi_2}{\varphi_2 - \varphi_1}\right)$$

4.2.5 Forces in a horizontal side bend

From Aadnoy and Andersen

Lowering	$F_2 = \frac{1}{2}\left[\left(F_1 + \sqrt{F_1^2 + (wR)^2}\right)e^{\mu(\alpha_2-\alpha_1)} - \frac{(wR)^2}{\left(F_1 + \sqrt{F_1^2 + (wR)^2}\right)e^{\mu(\alpha_2-\alpha_1)}}\right]$
Hoisting	$F_2 = \frac{1}{2}\left[\left(F_1 + \sqrt{F_1^2 + (wR)^2}\right)e^{\mu(\alpha_2-\alpha_1)} - \frac{(wR)^2 e^{\mu(\alpha_2-\alpha_1)}}{\left(F_1 + \sqrt{F_1^2 + (wR)^2}\right)}\right]$
Torque	$T_2 = T_1 + \mu r\lvert\alpha_2 - \alpha_1\rvert\sqrt{F_1^2 + (wR)^2}$

Table 4.7 Forces in a side bend

These are assuming that the weight of pipe in the side bend is also contributing to total side force.

4.2.6 The new 3D model for curved segments only

Hoisting and Lowering Curved	$F_2 = F_1 e^{\pm\mu\lvert\theta_2-\theta_1\rvert} + w\Delta TVD$
Torque curved	$T_2 = T_1 + \mu r F_1 \lvert\theta_2 - \theta_1\rvert$

Table 4.8 Summary of the new 3D model

4.2.7 New 3D model and combined motion

Straight lowering	$F_2 = F_1 + w\Delta L\cos\varphi - \mu w\Delta L\sin\varphi\sin\Psi$
Straight hoisting	$F_2 = F_1 + w\Delta L\cos\varphi + \mu w\Delta L\sin\varphi\sin\Psi$
Curved lowering	$F_2 = F_1 + F_1\left(e^{-\mu(\theta_2-\theta_1)} - 1\right)\sin\Psi + w\Delta TVD$
Curved hoisting	$F_2 = F_1 + F_1\left(e^{-\mu(\theta_2-\theta_1)} - 1\right)\sin\Psi + w\Delta TVD$
Angle of friction vector	$\Psi = \tan^{-1}\left(\frac{V_h}{V_r}\right) = \tan^{-1}\left(\frac{V_h\,60}{2\pi r RPM}\right) =$
Torque in straight	$T_2 = T_1 + \mu r w\Delta L\sin\varphi\cos\Psi$
Torque in bend	$T_2 = T_1 + \mu r F_1\lvert\theta_2 - \theta_1\rvert\cos\Psi$

Table 4.9 Combined motion with high string tension

In the 3D model for curved segments an assumption is made that the string is weightless, to find an expression for effect of tension, and then adds the weight of the string to the final result.

4.3 Critique of the new analytical 3D model

The new model has very simple formulation, which allows for quick computation time. When the tension is so high that the side force due to tension is a lot greater than the side force due to the weight of the pipe, the new 3D model works great. When tension is high it matches field data as shown by Mirhaj (2010), however, he also showed that the model gives an under prediction of friction in the lowest part of the string which has low tension. The reason for this under prediction can be seen by examining equation for the new model:

$$F_2 = F_1 e^{\pm\mu|\theta_2-\theta_1|} + w\Delta TVD \tag{69}$$

We see that if there is a horizontal side bend, the equation will be reduced to:

$$F_2 = F_1 e^{\pm\mu(\theta_2-\theta_1)} \tag{70}$$

When tension is low, the position of the string in the wellbore will be given by the sum of the gravity vector and the side force vector due to the bend. But the side force due to the weight of the pipe itself is ignored. In a horizontal side bend as shown in Figure 4.4 the pipe in the hole will lie on one sidewall if the tension is high. On the other hand, if there is no tension, the pipe will be gravity dominated and lies on the low side of the hole. The problem of under prediction of drag in a horizontal section with low tension was solved by Mirhaj (2010), he introduced a new tension criteria. In the criteria drag could be calculated by straight segment equation when the tension is low. With the new criteria more drag was predicted in the part of the string with low tension. But then the string is assumed to be on the low side when tension is low, and on the side of the wall when tension is above the critical limit. But in reality the string will be positioned somewhere in between these two extremes.

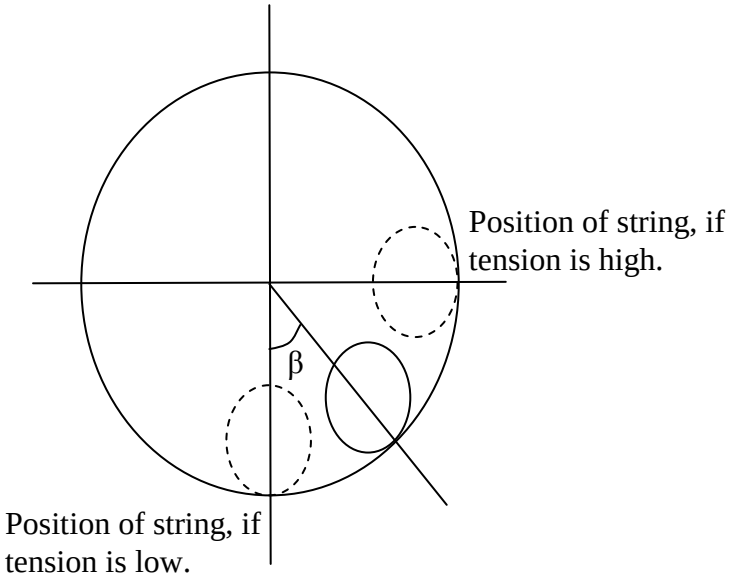

Figure 4.4 String position in a borehole.

So clearly the new model has some inaccuracies for the lowest part of the string where tension is low. It is worth noting that the side force effect of the string weight will be reduced the higher the pipe lies on the borehole wall. When a string is in the 3 or 9 o'clock position, the effect of the string weight on side force will be zero. This is shown in Figure 4.5, where the normal force due to gravity is greatest for the pipe on the low side.

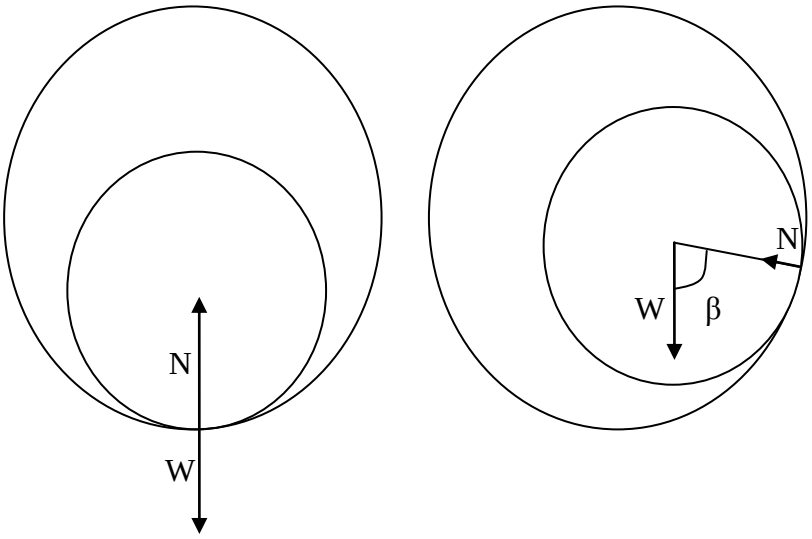

Figure 4.5 Forces due to gravity on horizontal pipe.

4.4 Proposed new model

To improve upon the deficiency when the tension is low we try to have a different approach to the problem. We consider an element of pipe and decompose the tension vector from previous segment into its horizontal and vertical components by using trigonometry. Then use the exact analytical equations for a horizontal side bend and the new 3D model is used in 2D for the vertical bend. By 2D we mean that for the vertical bend, only the change in inclination is considered. As it can be seen from 4.6 the side C can be decomposed into its horizontal component b, and its vertical component a. Note that the lines in the triangle are curved as if it is on the surface of a sphere.

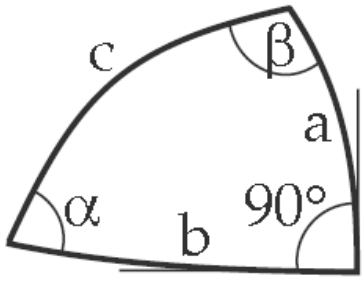

Figure 4.6 A triangle on a sphere.

Remembering that the most common well path model the "minimum curvature method" assumes the well path to be wrapped around the surface of a sphere, which is the largest sphere possible that will fit between the survey points. In other words, the sphere has "minimum curvature". This is shown in Figure 4.7, where the largest sphere g, fits in between survey station A and B.

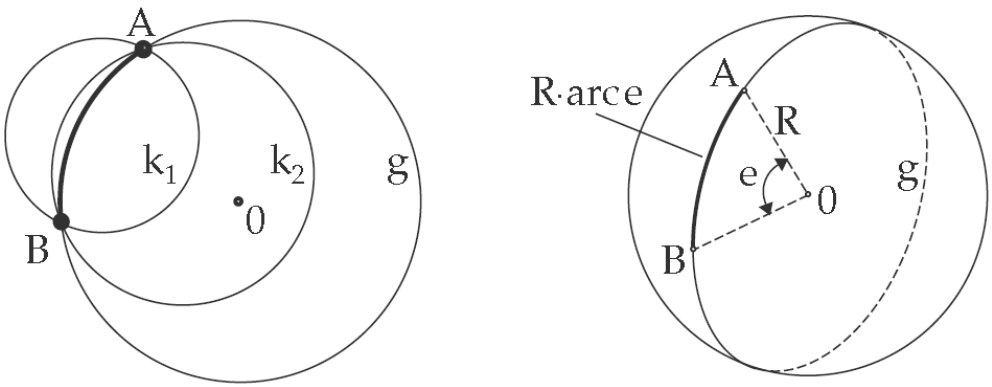

Figure 4.7 Minimum curvature method.

Since the radius of the sphere is a lot larger than the length between two survey stations, we may simplify slightly and use the Pythagorean theorem, instead of using more involved spherical trigonometry.

The horizontal component can be found by:

$$F_{\alpha,i} = F_{2,i-1} \cos\left(arctan\left(\frac{\Delta\varphi}{\Delta\alpha}\right)\right) \tag{71}$$

The vertical component can be found by:

$$F_{\varphi,i} = F_{2,i-1} \sin\left(\arctan\left(\frac{\Delta\varphi}{\Delta\alpha}\right)\right) \tag{72}$$

Then both the vertical and horizontal drag forces can be calculated individually. The vertical component on top of the element $F_{\varphi,2}$, and the horizontal component on top of the element $F_{\alpha,2}$. The net force on top of the segment F_2 is then calculated by re-combining using Pythagorean theorem and adding a term for the weight of the pipe:

$$F_2 = \sqrt{{F_{\varphi,2}}^2 + {F_{\alpha,2}}^2} + w\Delta TVD \tag{73}$$

Likewise this process will be repeated for the next upper element. The flowchart in Figure 4.8 shows how the model selects which equations that should be used.

This method of decomposing the force into its horizontal and its vertical components based solely on the change in inclination and azimuth is not an exact method. Some errors will be introduced when decomposing and recombining the forces. Trying to model a whole well by this method can be done, but the error introduced will be

greater. There is no reason for doing that because when tension is high, the effect of pipe weight can be ignored, and the new Aadnoy 3D model works well then. So this method is proposed to be used only where the side force due to the weight of the string is not to be ignored, that is when the string has low tension. This method is a better solution, than assuming that straight segment equations can be used.

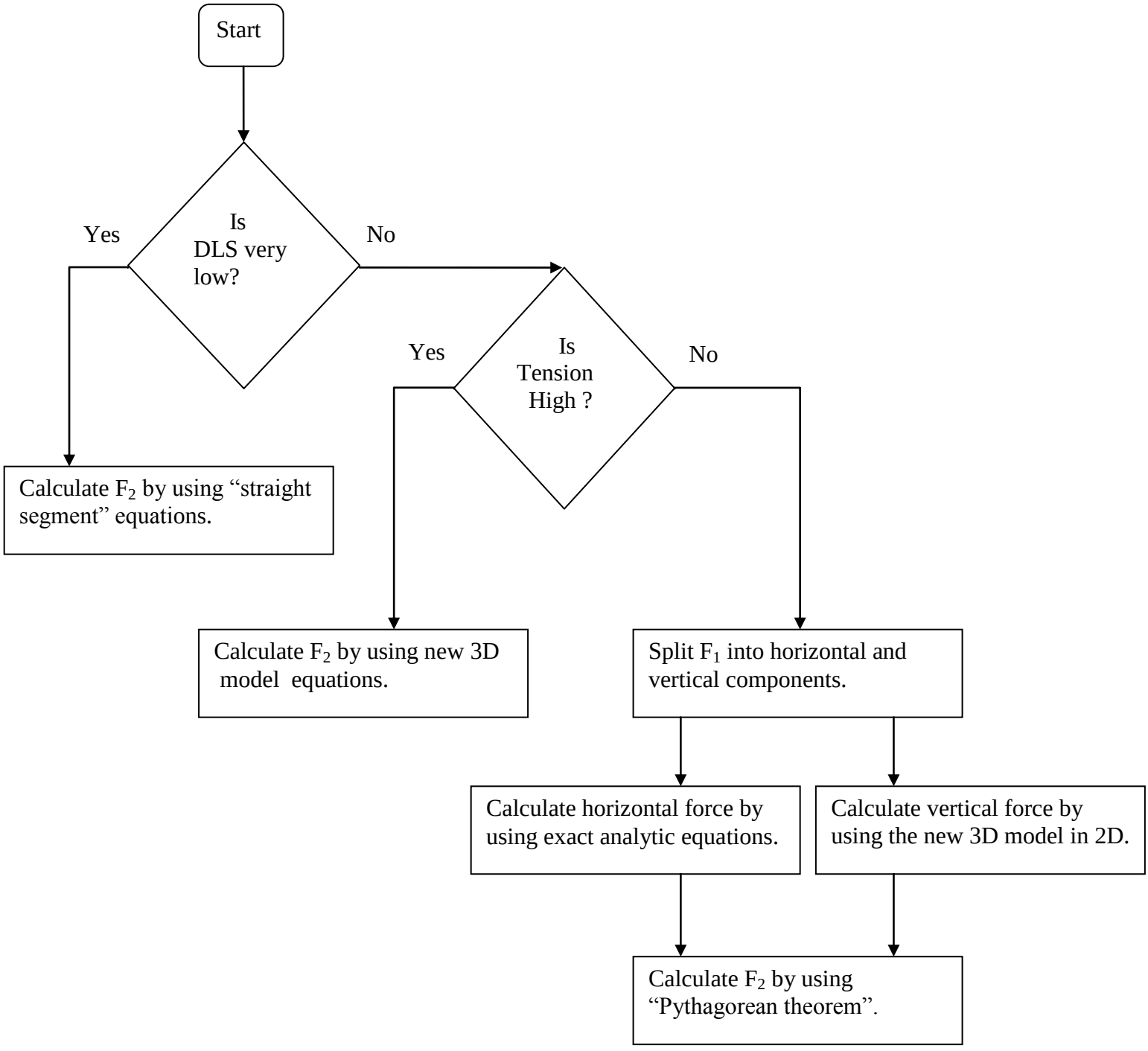

Figure 4.8 Flowdiagram showing how to calculate tension on top of a segment.

4.5 Straight or curved

A problem arises when we shall select which equation has to be used when the hole is almost straight. If a segment of the hole is perfectly straight, then we know we should use the equations for friction in a straight hole. But when the hole is close to straight we could still use straight segment equations. If the hole segment is more curved we know we should use equations for curved segments. We then have to find criteria for when we should use straight segment equation and when to use equations for curved segments.

4.5.1 Previous straightness criteria

Previous work with this new model has used several different criteria to determine if a segment is curved or straight. The latest version that is used compares the dogleg to a fixed dogleg limit, e.g. 0.05 radians. For any dogleg greater than this limit and curved segment equations should be used. The method used to find this curvature limit can certainly be debated since the selection of the curvature limit has an impact on the modeled results. Previous work have used field data to set the curvature limit for each specific well so that straight tangent sections are modeled as straight and any build sections are modeled as curved.

The tension is also checked so that when the tension is lower than a certain limit, then straight segment equations are used. This is illustrated in Figure 4.9. The high tension limit should also be based on field data for the specific well. There is no specific right way of finding the tension limit. Several methods could be used. Mirhaj (2010) derived an equation for the tension limit:

$$F_{limit} = \frac{\overline{w}_{BHA}\overline{\Delta L}\sin\varphi}{2\sin\left(\frac{\bar{\theta}}{2}\right)} \tag{74}$$

Where $\overline{w}_{BHA}$ is the average unit weight of the BHA, since it is most critical at the bottom of the well. $\overline{\Delta L}$ is the average distance between surveys, and the average dogleg is $\bar{\theta}$.

A different approach to find the critical tension limit is to calculate ratio between the side force due the weight of the pipe, and side force due to tension and curvature. By plotting this ratio we can set the tension limit to the tension in the string where the ratio starts to increase. That is where the side force due to tension is starting to be dominating over side force due to the weight of the string, for a specific segment. This ratio can be found by:

$$R = \frac{w\Delta L\sin\varphi}{F\theta} \tag{75}$$

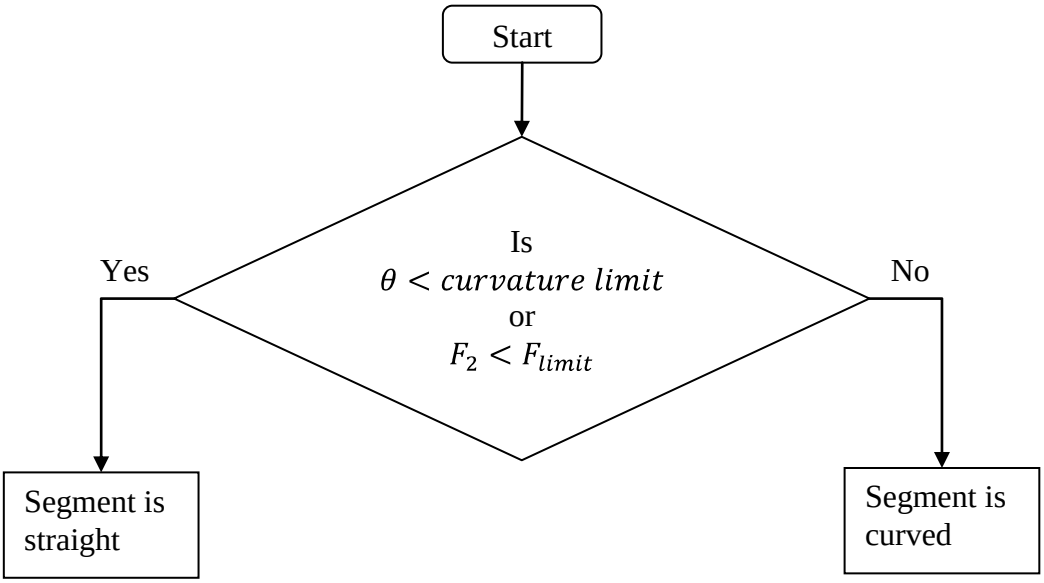

Figure 4.9 Latest criteria for determining if segment is straight or curved

4.5.2 DLS filter

A different criterion for determining whether a segment is straight or curved, would be to use a dogleg severity filter, DLS filter. This filter will then use the radius of the curve as well as the radius for the segments above and below. Then the distance, h, from a reference line is calculated, ref. Figure 4.10.

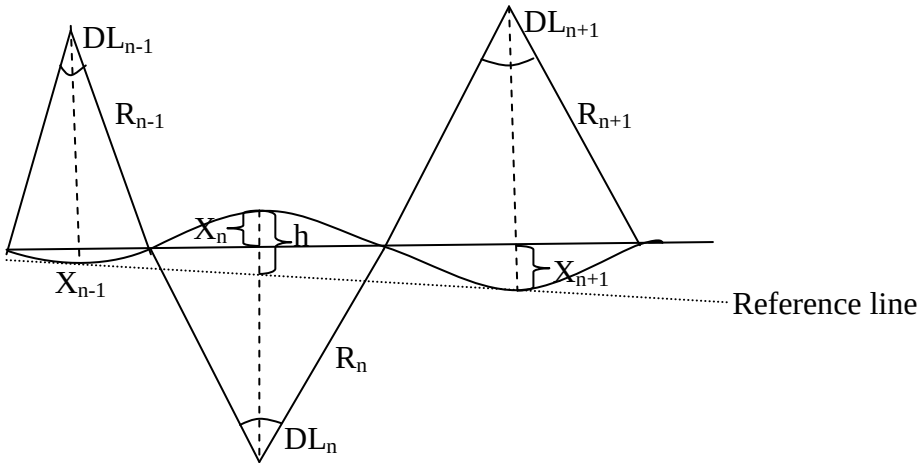

Figure 4.10 DLS filter.

Then this distance is compared to the radial clearance between the string and borehole, ref. Figure 4.11. If radial clearance is less than the distance from the reference line, we would use curved equations. And if clearance is greater we would use straight equations.

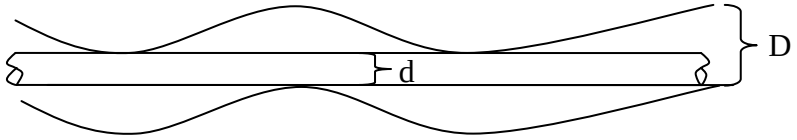

Figure 4.11 Pipe in a curved wellbore.

First we calculate the radius of the 3 segments:

$$R_{n-1} = \frac{\Delta L_{n-1}}{DL_{n-1}} \tag{76}$$

$$R_n = \frac{\Delta L_n}{DL_n} \tag{77}$$

$$R_{n+1} = \frac{\Delta L_{n+1}}{DL_{n+1}} \tag{78}$$

Then we find the heights:

$$X_{n-1} = R_{n-1}\left(1 - \cos\left(\frac{DL_{n-1}}{2}\right)\right) \tag{79}$$

$$X_n = R_n\left(1 - \cos\left(\frac{DL_n}{2}\right)\right) \tag{80}$$

$$X_{n+1} = R_{n+1}\left(1 - \cos\left(\frac{DL_{n+1}}{2}\right)\right) \tag{81}$$

The total deviation from the reference line will then be approximately:

$$h \cong \frac{1}{2}(X_{n-1} + X_{n+1}) + X_n \tag{82}$$

Then we can compare this deviation to the radial clearance between string and casing:

If $h < (D - d)$ then assume the segment to be straight.

If $h > (D - d)$ then assume the segment to be curved.

5 Field case study

5.1 Introduction to the example well

The well has been selected for the case study is a horizontal well drilled in the North sea. It was drilled from a Jack up rig to TD at 6015 m MD. A 13 5/8" casing was set to 1730 m MD. And a 10" liner was set from 1701m MD to 4501 m MD. A well schematic with the 8.5" drilling assembly is shown in Figure 5.1.

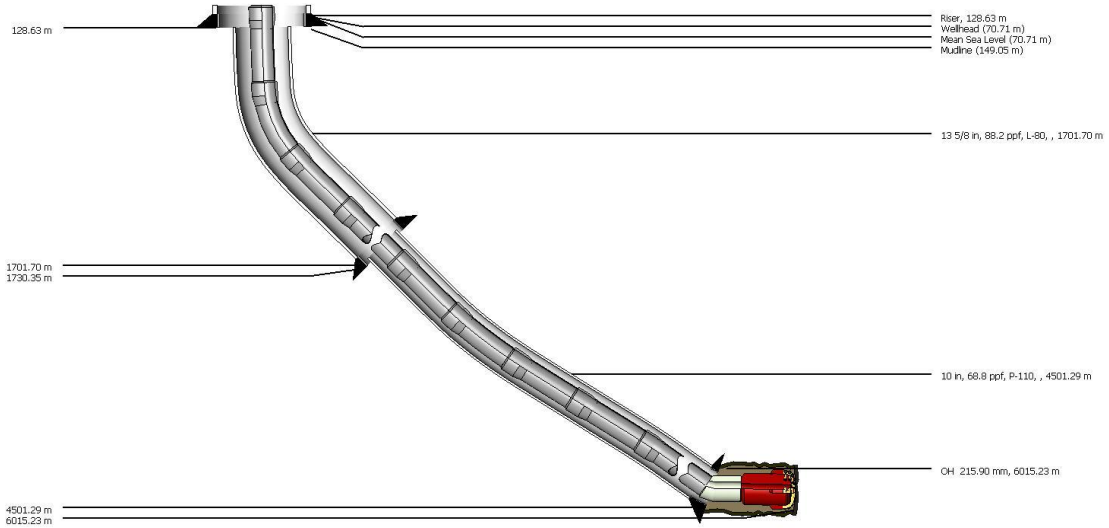

Figure 5.1 Field case well schematic.

This well builds angle three times:

1. The first KOP 600 m.
2. The second at 2000 m TVD.
3. Final build to horizontal at 3200 m TVD.

As shown in the vertical section in Figure 5.2 and in the inclination graph in Figure 5.3

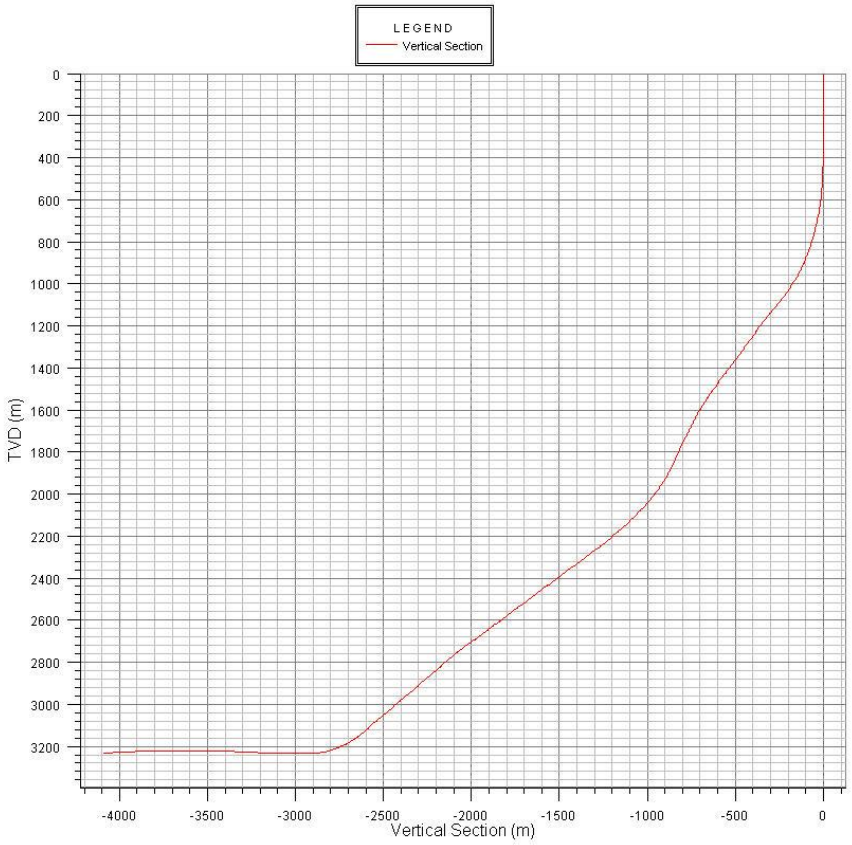

Figure 5.2 Field case, vertical section.

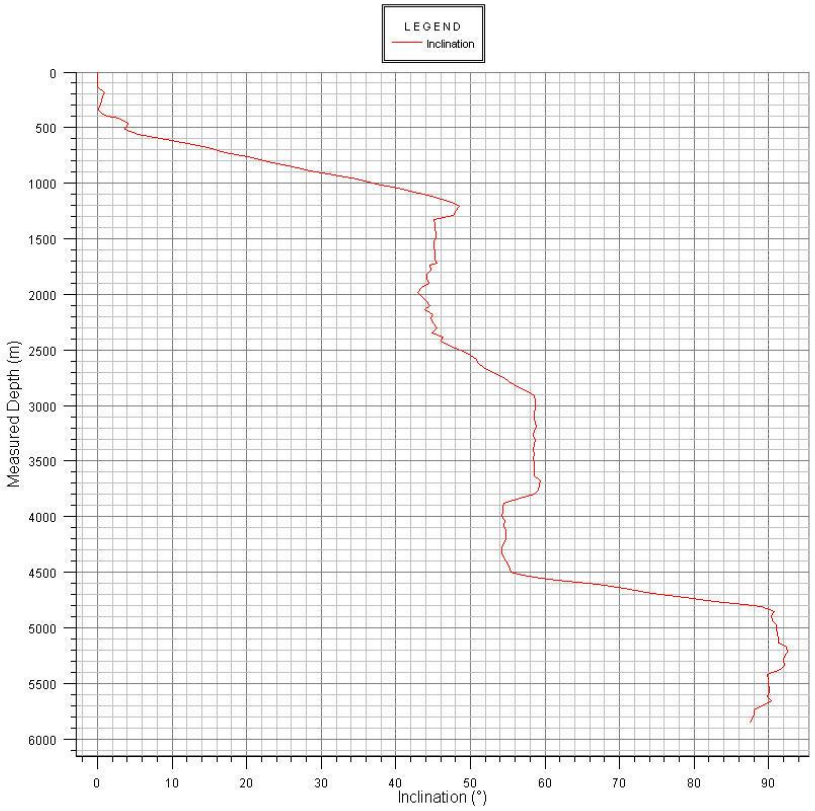

Figure 5.3 Field case, inclination vs. depth.

This well also has three large turns in azimuth, as shown in the departure in Figure 5.4 and in the azimuth graph in Figure5.5.

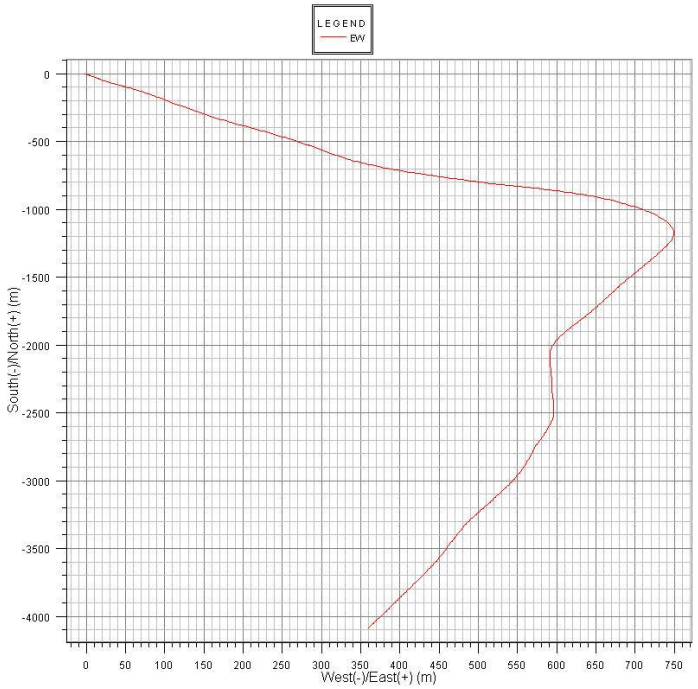

Figure 5.4 Field case, departure.

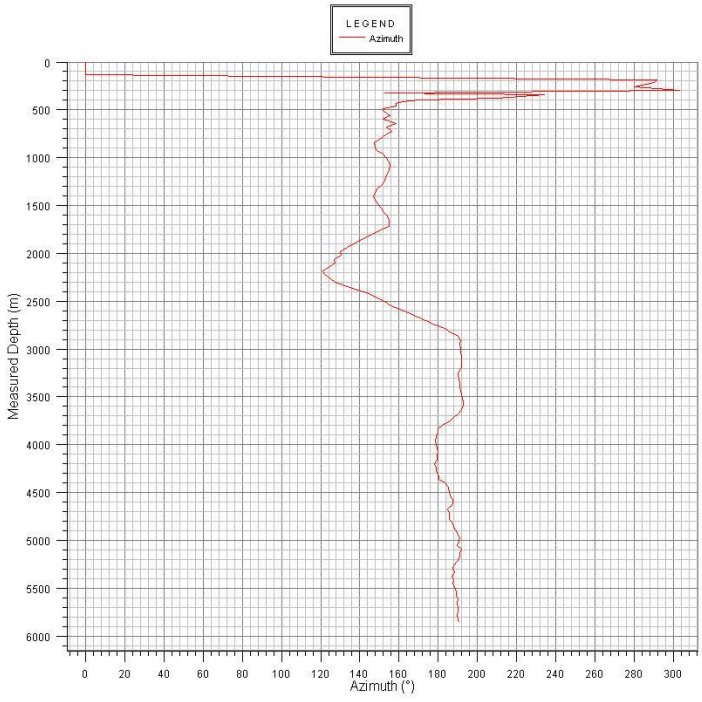

Figure 5.5 Field case, azimuth vs. depth.

The dogleg severity in this well is not very large, with a maximum of 4 deg/30m at 4600 m MD, as shown in Figure 5.6.

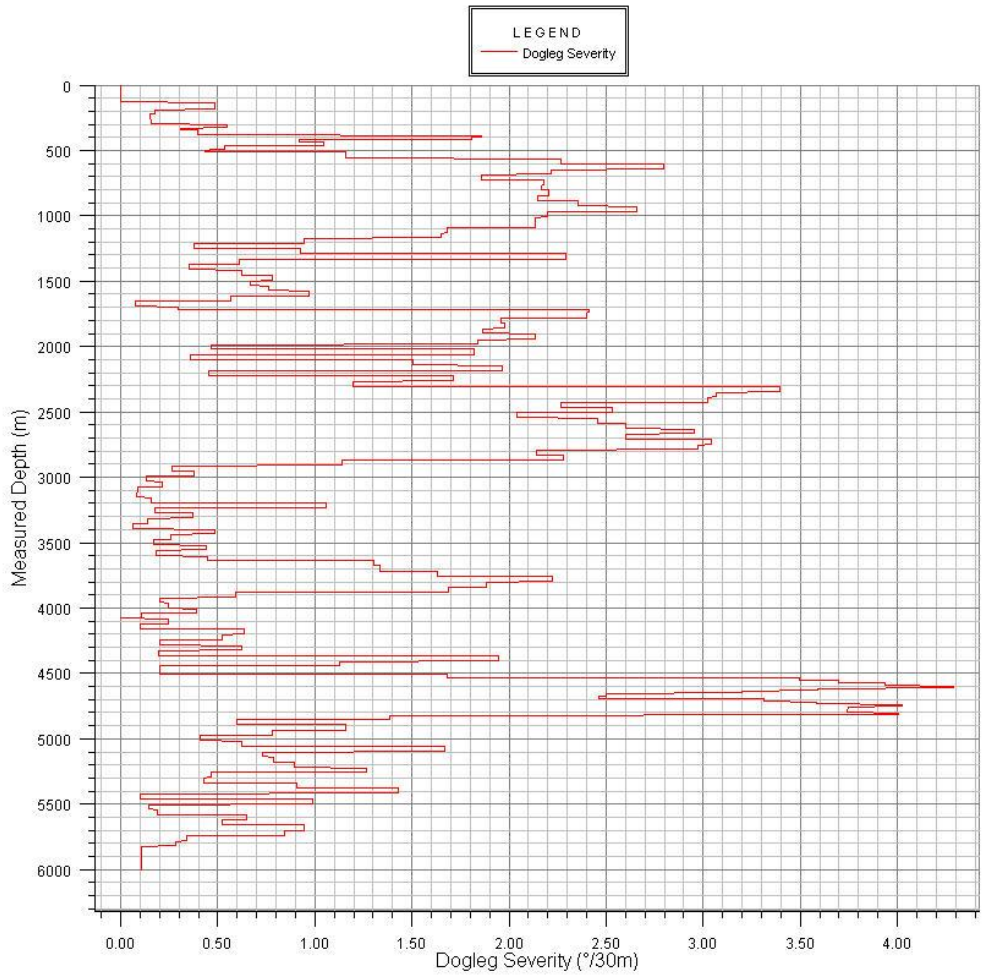

Figure 5.6 Field case, doglegseverity.

The drill string and borehole used in all simulations are the same as the one that was used in Wellplan as shown in Figure 5.7.

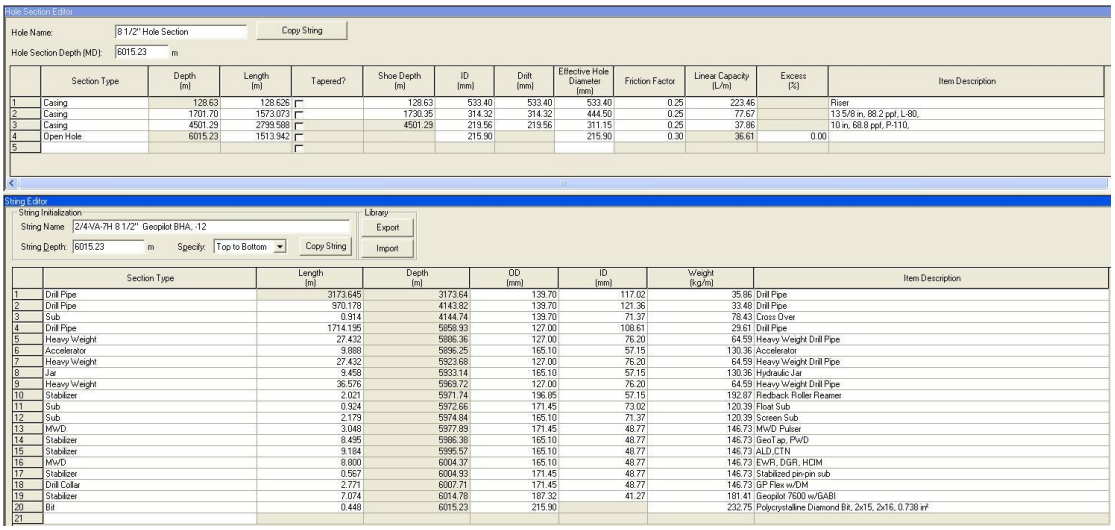

Hole Section Editor

Hole Name: 8 1/2" Hole Section — Copy String

Hole Section Depth (MD): 6015.23 m

	Section Type	Depth (m)	Length (m)	Tapered?	Shoe Depth (m)	ID (mm)	Drift (mm)	Effective Hole Diameter (mm)	Friction Factor	Linear Capacity (L/m)	Excess (%)	Item Description
1	Casing	128.63	128.626	☐	128.63	533.40	533.40	533.40	0.25	223.46		Riser
2	Casing	1701.70	1573.073	☐	1730.35	314.32	314.32	444.50	0.25	77.67		13 5/8 in, 88.2 ppf, L-80,
3	Casing	4501.29	2799.588	☐	4501.29	219.56	219.56	311.15	0.25	37.86		10 in, 68.8 ppf, P-110,
4	Open Hole	6015.23	1513.942	☐		215.90		215.90	0.30	36.61	0.00	
5				☐								

String Editor

String Initialization — String Name: 2/4-VA-7H 8 1/2" Geopilot BHA, -12 — String Depth: 6015.23 m — Specify: Top to Bottom — Copy String

Library — Export — Import

	Section Type	Length (m)	Depth (m)	OD (mm)	ID (mm)	Weight (kg/m)	Item Description
1	Drill Pipe	3173.645	3173.64	139.70	117.02	35.86	Drill Pipe
2	Drill Pipe	970.178	4143.82	139.70	121.36	33.48	Drill Pipe
3	Sub	0.914	4144.74	139.70	71.37	78.43	Cross Over
4	Drill Pipe	1714.195	5858.93	127.00	108.61	29.61	Drill Pipe
5	Heavy Weight	27.432	5886.36	127.00	76.20	64.59	Heavy Weight Drill Pipe
6	Accelerator	9.888	5896.25	165.10	57.15	130.36	Accelerator
7	Heavy Weight	27.432	5923.68	127.00	76.20	64.59	Heavy Weight Drill Pipe
8	Jar	9.458	5933.14	165.10	57.15	130.36	Hydraulic Jar
9	Heavy Weight	36.576	5969.72	127.00	76.20	64.59	Heavy Weight Drill Pipe
10	Stabilizer	2.021	5971.74	196.85	57.15	192.87	Redback Roller Reamer
11	Sub	0.924	5972.66	171.45	73.02	120.39	Float Sub
12	Sub	2.179	5974.84	165.10	71.37	120.39	Screen Sub
13	MWD	3.048	5977.89	171.45	48.77	146.73	MWD Pulser
14	Stabilizer	8.495	5986.38	165.10	48.77	146.73	GeoTap, PWD
15	Stabilizer	9.184	5995.57	165.10	48.77	146.73	ALD,CTN
16	MWD	8.800	6004.37	165.10	48.77	146.73	EWR, DGR, HCIM
17	Stabilizer	0.567	6004.93	171.45	48.77	146.73	Stabilized pin-pin sub
18	Drill Collar	2.771	6007.71	171.45	48.77	146.73	GP Flex w/DM
19	Stabilizer	7.074	6014.78	187.32	41.27	181.41	Geopilot 7600 w/GABI
20	Bit	0.448	6015.23	215.90		232.75	Polycrystalline Diamond Bit, 2x15, 2x16, 0.738 in²
21							

Figure 5.7 Field case, drillstring and borehole.

This example well was drilled with Halliburton ADT service which used Landmark's Wellplan software for simulating torque and drag in order to monitor the hole conditions by comparing actual field measured hookload and torque with the model. Very consistent hookload data was measured for hoisting, lowering and static weight, as well as free rotating torque. These measurements were done at every stand before a new connection was made. The measured hookloads for lowering, static and hoisting are plotted and the model in wellplan was first tuned to match the static weight, and then to hoisting and lowering weights. A combined plot shows the measured weight and the wellplan model for both the 12.25" section and the 8.5" section in Figure 5.8 The sudden jump at 4500 m is due to a lighter BHA was used to drill the lowest section. This is due to 8" MWD tools were used in the 12.25" section, while in the 8.5" section the smaller 6 ¾" MWD tools were used.

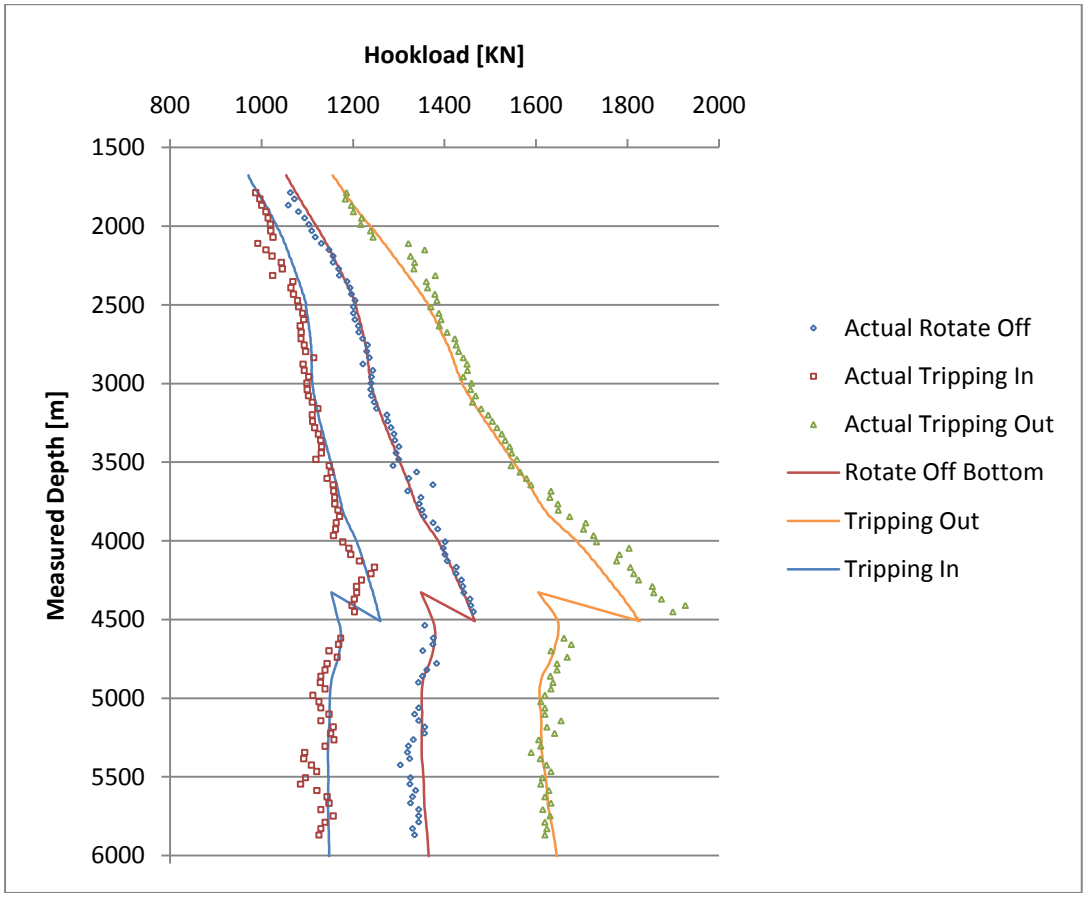

Figure 5.8 From wellplan, drilling 12,25" and 8,5"

5.2 Wellplan torque and drag module

The equations used in calculating torque and drag in Wellplan are based on the model presented by Johancik et al. This model is sometimes referred to as the Standard model in this thesis. This model is referred to as "Exxon model" too, since Johancik had been developing the model for Exxon acquirement at that time. Comparison between the Wellplan calculated results and our "Exxon" model was performed. The Figure 5.9 shows that for the 8.5" section, when Wellplan and our "Exxon" model is given the same inputs, the calculated results is almost the same. The small differences, are probably due to small rounding errors in specifying the drill string weights and lengths. The 3D model is also shown, and we see that they all give almost the same results.

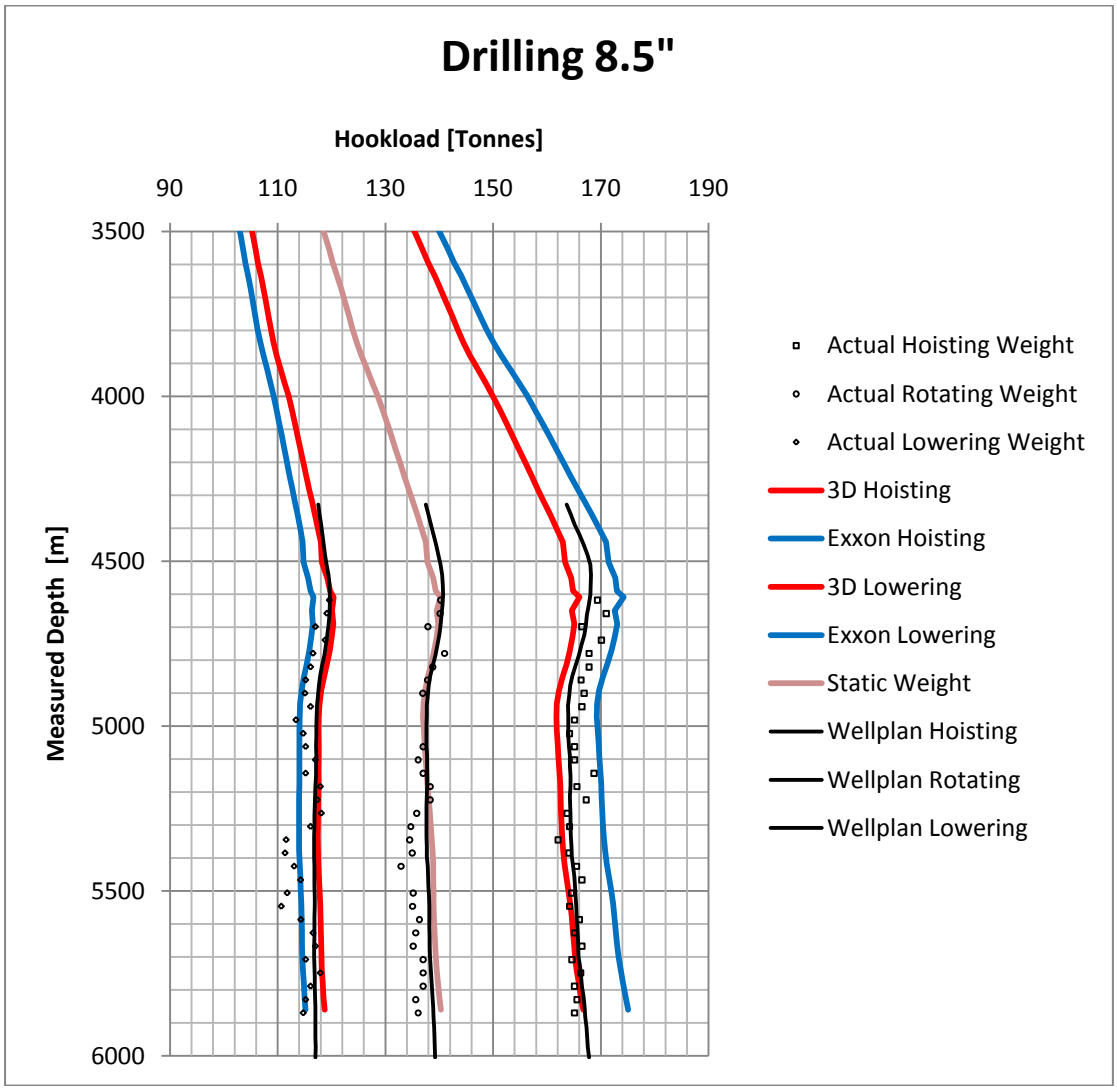

Figure 5.9 Comparison between Wellplan and Exxon model.

5.3 Sheave friction

It is possible to tune the models so that we get a good match between field measured data for hoisting, lowering and static weight. However, the method used to tune the model can rise to questions. Firstly the "static weight" off bottom is not dependent on friction factor, but only on unit weight of string, mud weight and vertical depth. So if measured static weight does not match the model, either wrong string weight has been entered to the model or the hookload sensor is out of calibration. The modelled static weight has to be tuned to match field data either by correcting the unit pipe weight or by calibrating the measured hookload. Secondly the hoisting and lowering weights are measured with moving sheaves in the crown and travelling block and are therefore affected by sheave friction. This means that the measured weight are actually a bit lower for hoisting and higher for lowering than it is in reality. Corrections for sheave friction may be applied either to the model or to actual measured data. In Figure 5.10, Wellplan is used for modelling of drilling in the 8.5" section. The model is matched to actual values but there is no correction for sheave friction. The friction factor to match is very low, 0.16 for lowering and 0.14 for hoisting. We might say that the sheave friction is then included in "fudge" of the friction factor. This might seem unrealistically low, but this is actually how the company who drilled this well tuned in their model.

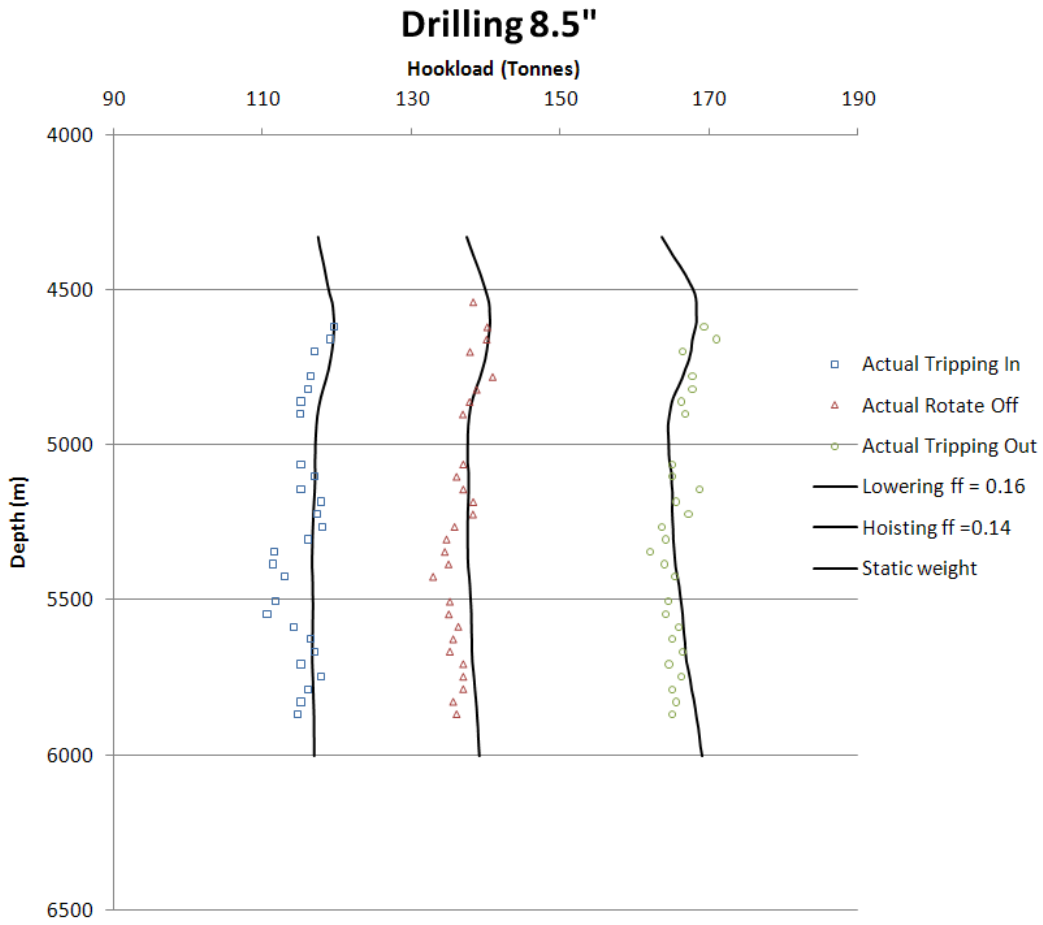

Figure 5.10 Matching actual data with no sheave friction correction.

This way of tuning in the drag model could without doubt been improved. But it comes down to what the model is used for and the quality of available data. In the

case of this well the main purpose was to monitor hole condition for signs of trouble like cutting accumulations and hole cleaning. Experience with many wells told them that they would only need to do remedial action whenever actual hookload deviated by more than 9 tonnes from the model. For this use the numeric value of the hookload is rather uninteresting, it is rather the trend and the sudden deviations from the trend that is the most interesting.

If we apply sheave friction correction to the model, the result is shown in Figure 5.11. In this case effect is that the curves for hoisting and lowering are shifted towards the static weight curve. More accurate data would need to be available to do an accurate calibration of the sheave efficiency, so in this case a typical (Luke 1993) sheave efficiency of 98% was used.

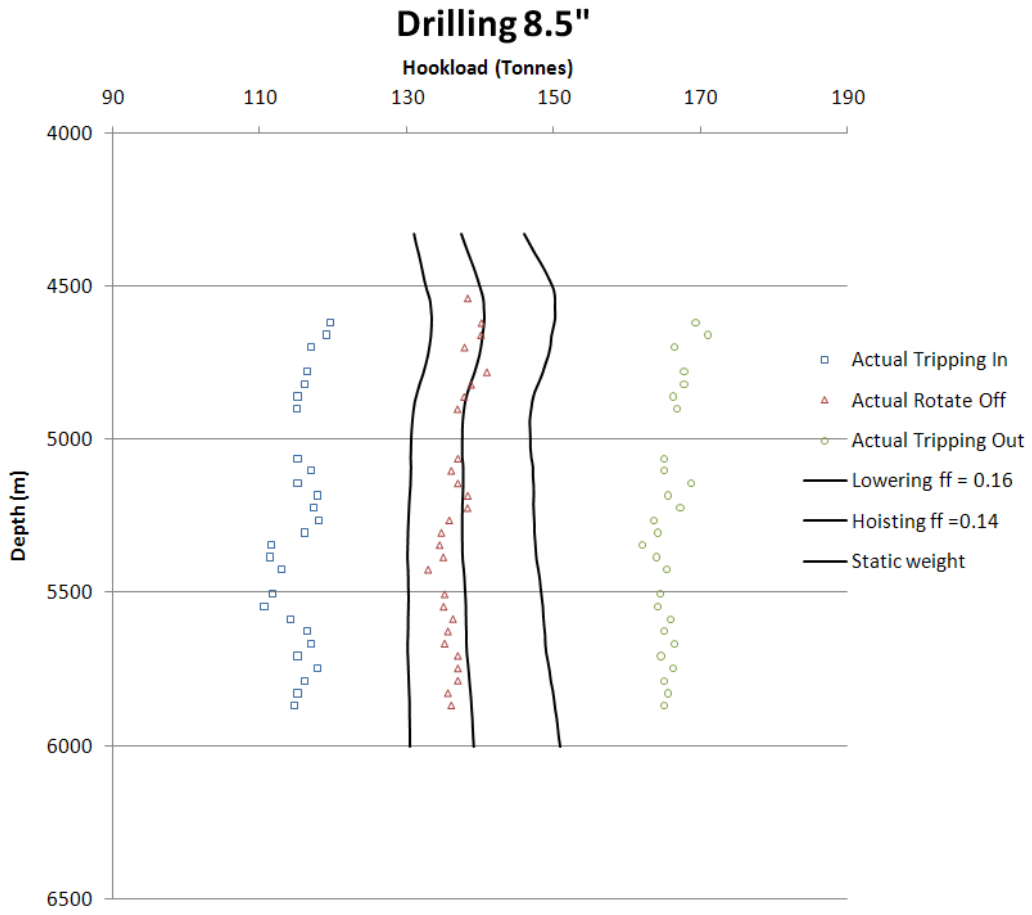

Figure 5.11 Sheave friction correction applied to the model.

If we now tune the friction factor, we can match the actual data by a higher and more realistic friction factor. In Figure 5.12 the actual data are matched by a friction factor of 0.28 for hoisting and 0.21 for lowering. This shows that the effect of sheave friction is something that we need to consider. Even though sheave efficiency is rather difficult to determine accurately.

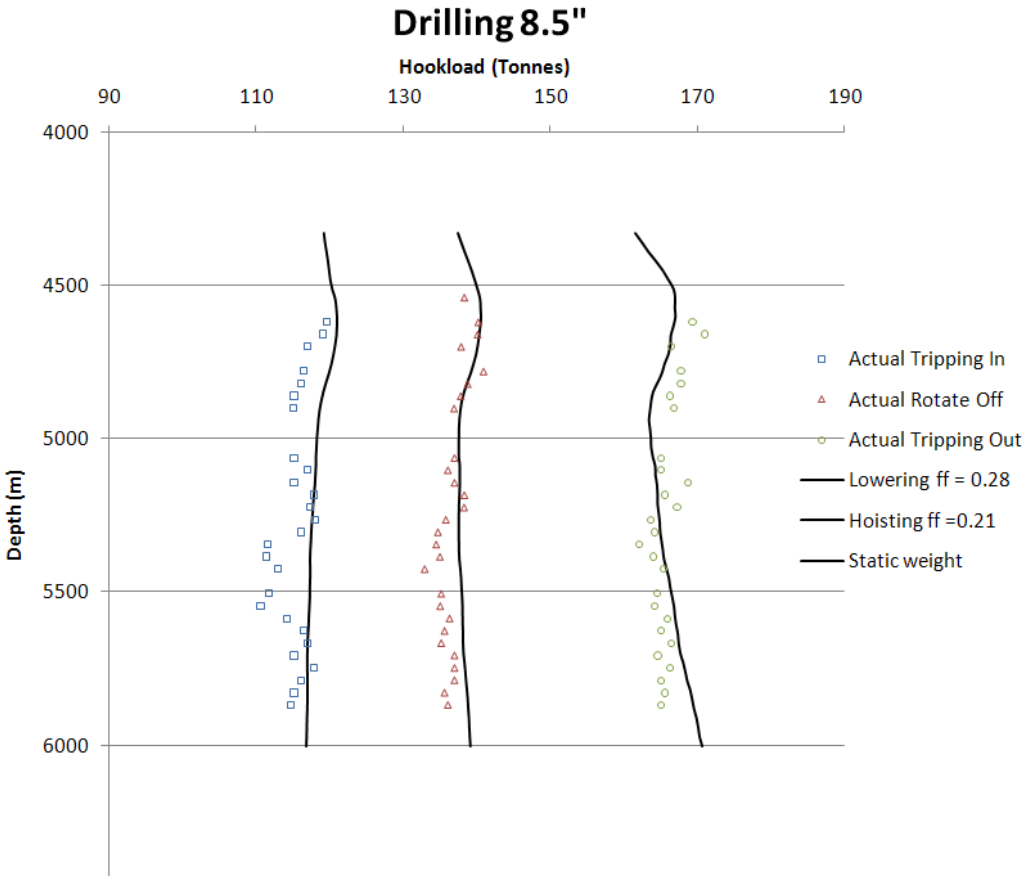

Figure 5.12 Matching the actual data with sheave friction correction and higher more realistic friction factors.

5.4 DLS filter as straightness criteria

It was tested to see how the newly proposed DLS filter would perform. The same field case well was used, this time it was tested only with Aadnoy's new 3D model for hoisting. This test was done with the standard straight/curved criteria and the new DLS filter. The Figure 5.13 shows the tension in the string for hoisting with bit close to TD. The blue vertical line shows when the standard criterion gives the segment as "straight". The red vertical line shows when the DLS filter gives the segment as "straight". We see that the new DLS filter gives that a segment is "curved" a lot more than the standard criteria. The DLS filter gives that 30% of the segments are "straight", while the standard criteria give 81%. Even with such a great difference the calculated hookload through the string and at top is still very similar.

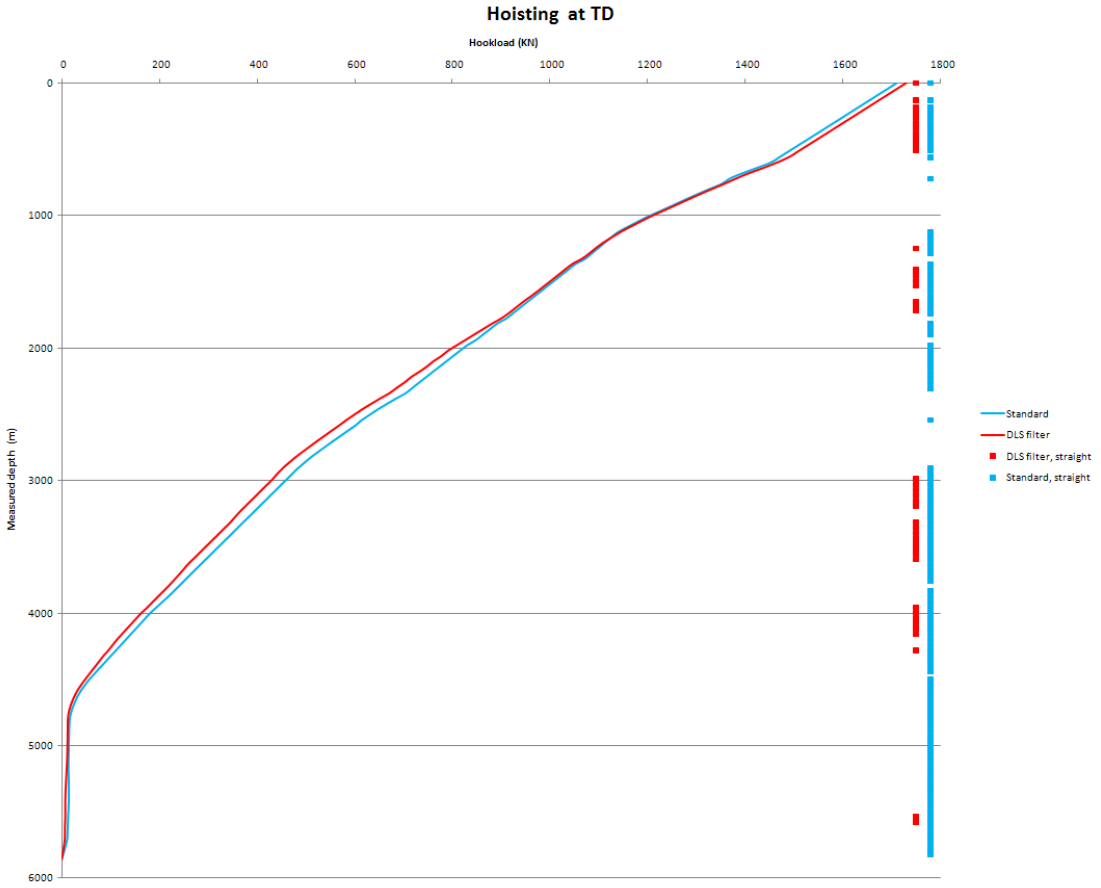

Figure 5.13 Hoisting close to TD, with the two different straightness criteria.

The next check was to see what the difference would be for a string being pulled out of hole POOH. What was done was essentially the calculations done to create 5.13, and repeat it again and again at increasingly shallower, to create a new curve for the hookload while POOH after drilling to TD in the 8.5" section as shown in Figure 5.14. What we see is that the standard criteria and the new DLS filter give very similar curves with only small differences. The actual measured hookload, recorded by engineers at every stand, seem to correlate well to both. Interestingly the recorded

hookload started to increase from 4330 m MD, this deviation from the model is most likely caused by a hole problem, such as e.g. cuttings accumulation.

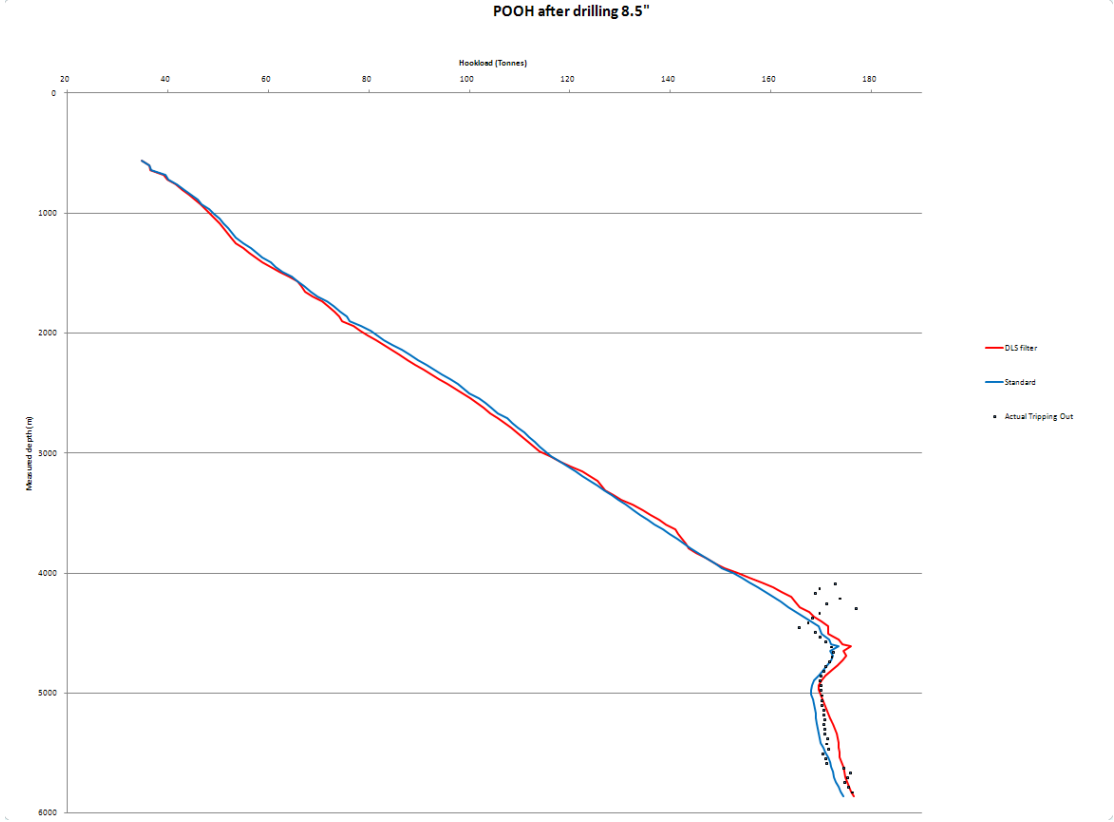

Figure 5.14 POOH after reaching TD.

5.5 New proposed model

It was tested to see how the new proposed model for low tension would perform. The same field case well was used, this time it was tested against Aadnoy's new 3D model for hoisting and lowering. This test was done with the standard straight/curved criteria for the 3D model, with a curvature limit of 0.03 radians and a tension limit of 700. This tension limit was found by calculating the ratio between side force due to weight of the pipe and side force due to the tension and curvature, by using equation (75). By examining Figure 5.15, we see that the side force ratio for hoisting is below 2 for the lower part of the string and then increases rapidly further up. This is where we should set the tension limit. A tension in the string of 700 KN is found where the ratio is 3 for both lowering and hoisting. Higher up the string the tension ratio is so much higher that the side force due to pipe weight is negligible as compared to the side force due to tension and curvature.

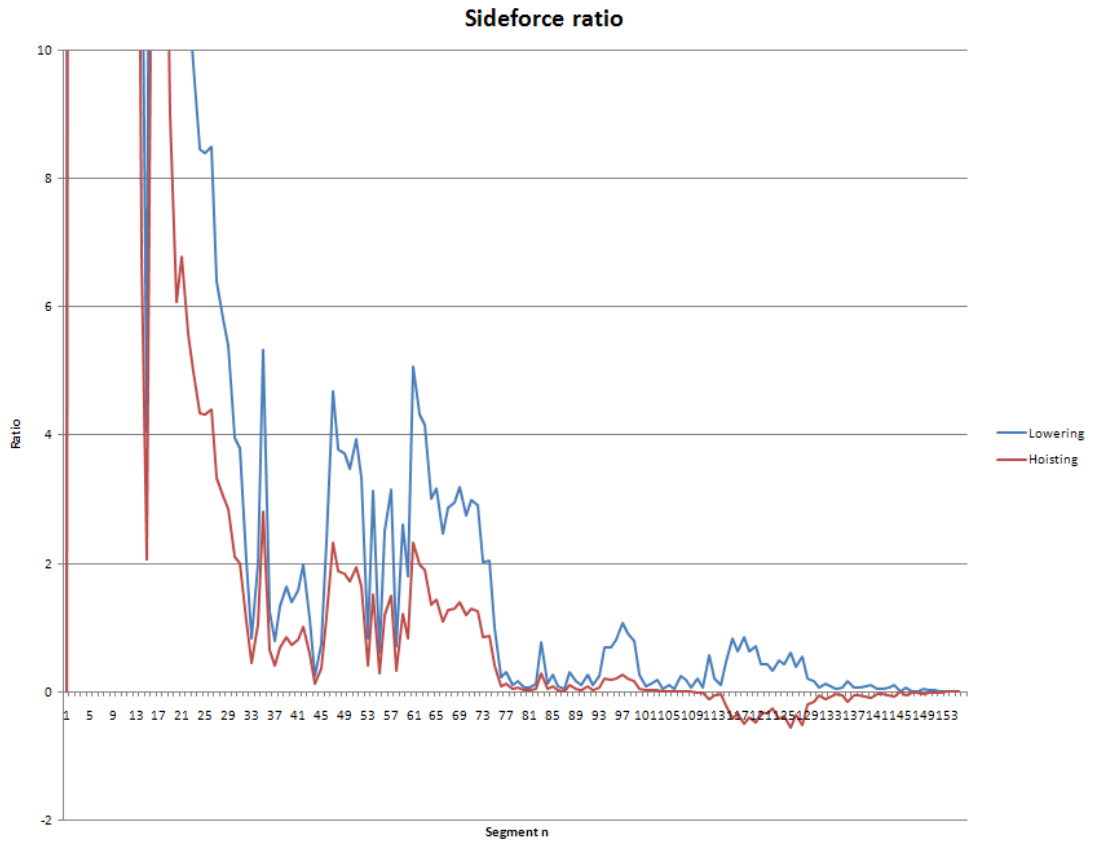

Figure 5.15 Side force ratio.

Figure 5.16 shows the tension in the string for hoisting and lowering with bit close to TD. The red dots shows segments where the new proposed model is used, green dots shows segments where straight line equations are used and blue dots shows segments where the new 3D model is used. We see that the curves for hoisting and lowering with new proposed model and the 3D model are overlapping and the results are very similar, except that the new proposed model gives slightly higher hookload for hoisting and slightly less hookload for lowering. This is as expected from theory since the new proposed model includes drag due to curvature and account for the position of the pipes position on the wellbore wall while the other model assumes straight line equations.

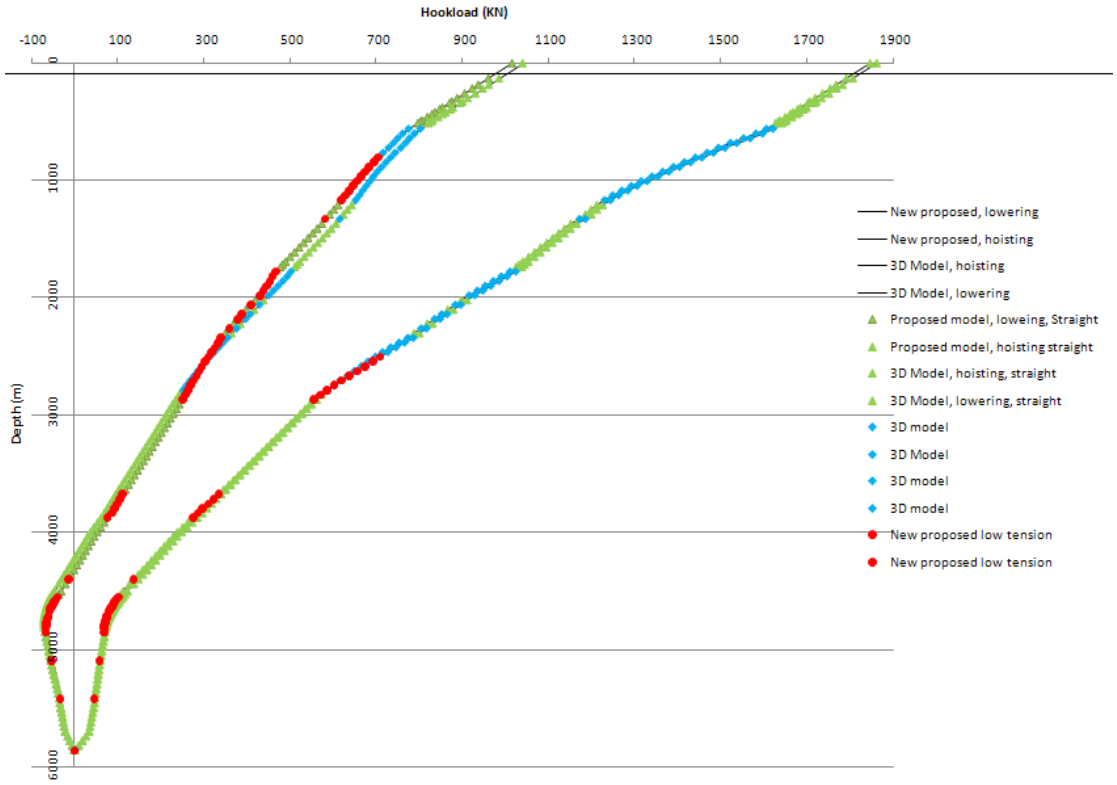

Figure 5.16 Hoisting and lowering with the new proposed model.

For POOH and RIH with the new proposed model, as shown in Figure 5.17 and Figure 5.18. We see that the calculated result is very similar for both models, except that the new proposed model predicts slightly less hookload for lowering while RIH, and predicts a slightly higher hookload for hoisting while POOH.

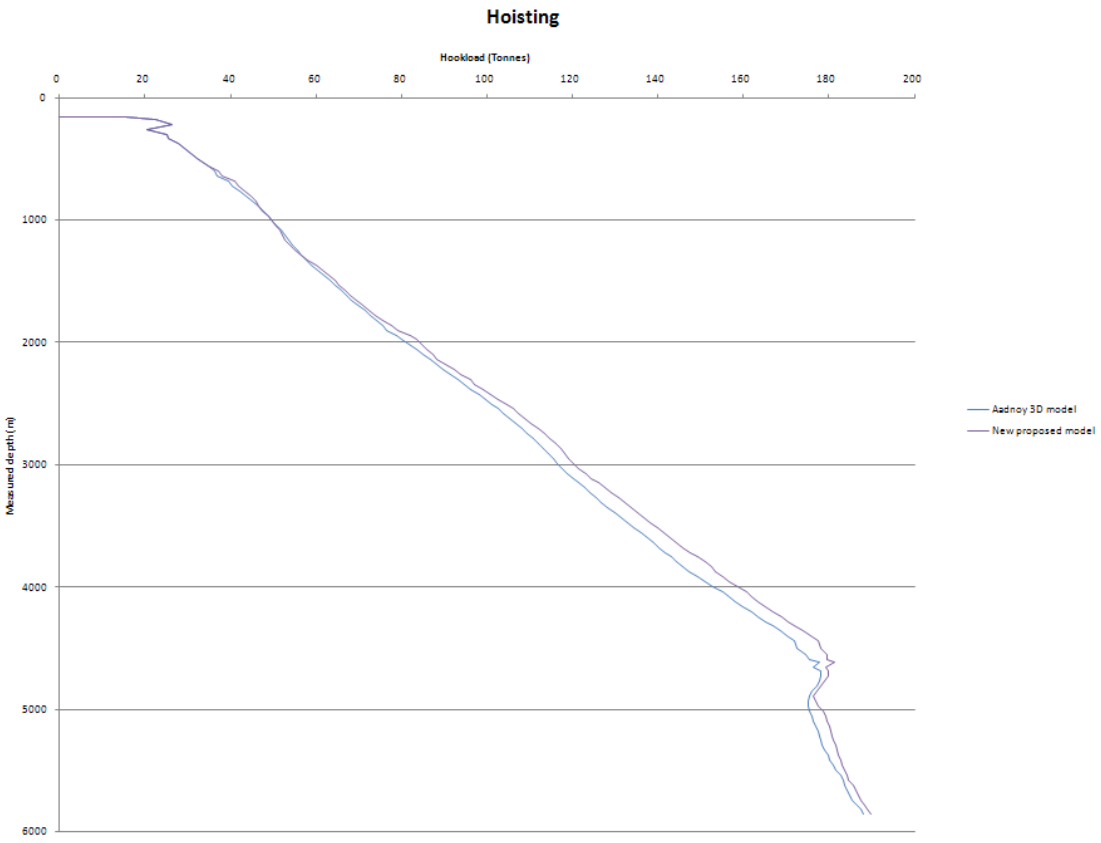

Figure 5.17 POOH with the new proposed model.

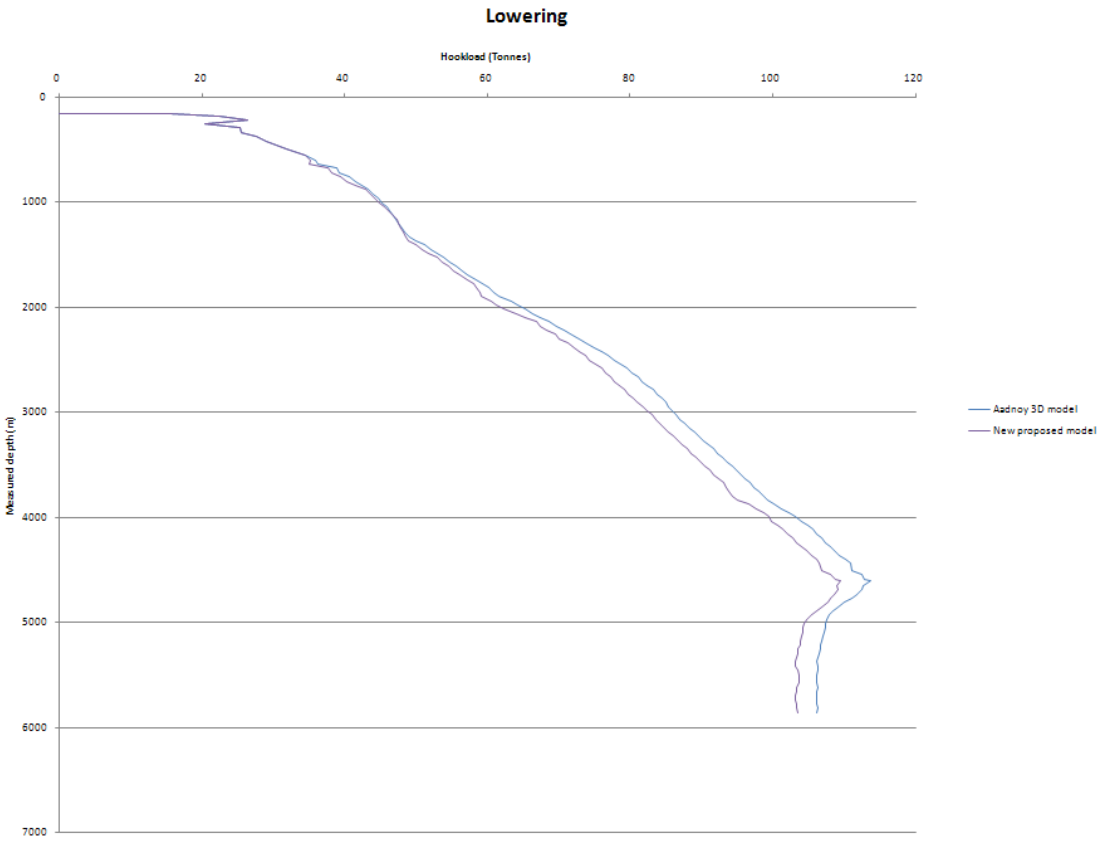

Figure 5.18 RIH with the new proposed model.

6 Conclusion

The following conclusion has been taken from this thesis:

- The new 3D model has some inaccuracy for the lower part of the string with low tension, since the side force due to the weight of the string is not accounted for. A new approach to this problem has been taken, and a new model is proposed and presented for the first time. This proposed model for the lowest part of the string, accounts for side force due to weight of the string, the position of the string in the borehole and the curvature in 3D. From the specific field case study, this new proposed model predicts slightly more drag than the previously used model.

- The new 3D model consists of two sets of equations for straight and curved wellbore sections. To set the limit for determining if a wellbore section is curved or straight can be troublesome, and it has an impact on the calculated result. Previous work with this model has used a straight/curved criterion which is based on a dogleg limit and a tension limit. This tension limit was based on side force due to tension and side force due to the weight of the string. A new approach to this problem has been taken and in this thesis a new straight/curved criterion is presented for the first time. This new criterion, the DLS filter, account for wellbore trajectory and the radial clearance between drill string and wellbore wall. From the specific field case study, the DLS filter gives more segments as curved, as compared to the previous model. However it only had a small effect on the calculated result. More studies on other well paths should be taken to further investigate the validity of the DLS filter.

- The friction factor is a lumped parameter which is dependent on many factors, not just true mechanical friction. Friction in the draw works sheaves affects the hoisting and lowering weights. It has been shown in the thesis how this effect can be corrected for. Some of the "fudge" in the friction factor can then be removed and a more realistic friction factor can be obtained.

7 References

Cayeux, E., Daireaux, B., “Early Detection of Drilling Condition Deterioration Using Real Time Calibration of Computer Models: Field Example from North Sea Drilling Operations” SPE/IADC 119435, Drilling and Conference Exhibition, Amsterdam, The Netherlands, March, 2009.

Fazaelizadeh, M., Hareland, G., Aadnoy, B.S. ”Application of New 3-D Analytical Model for Directional Wellbore Friction”, Journal of Modern Applied Science, Vol. 4, No. 2, 2010

Gaynor, T., Hamer, D., Chen, D., “Quantifying tortuosities by Friction Factors in Torque and Drag Model”, SPE 77617, Annual Technical Conference and Exhibition, San Antonio, Texas, September, 2002.

Johancsik, C.A., Friesen, D.B., Dawson, R. Torque and Drag in Directional Wells – Prediction and Measurement. June 1984

Luke, G.R., Juvkam-Wold, H.C., “Determination of true hookload and line tension under dynamic conditions” Journal of SPE Drilling and Completion, December, 1993.

Maehs, J., Renne, S., Logan, B., Diaz, N., “ Proven Methods and Techniques to Reduce Torque and Drag in the Pre Planning and Drilling Execution of Oil and Gas Wells”, IADC/SPE 128329, Drilling Conference and Exhibition, New Orleans, Lousiana, USA, February, 2010.

Maidla, E.E., Wojtanowicz, A.K., “Field method of assessing borehole friction for directional well casing” SPE Middle East Oil Show, Manama, Bahrain, March, 1987.

Manson, C.J. BP Exploration, Chen, D.C.K. Halliburton Sperry Services. Step Changes Needed To Modernize T&D Software. SPE/IADC 104609. 2007.

Mirhaj, S.A., Fazaelizadeh, M., Kaarstad, E., Aadnoy, B.S. “New Aspects of Torque and Drag Modelling in Extended Reach Wells”, SPE 135719, SPE Annual Technical Conference and Exhibition, Florence, Italy, September 2010.

Mirhaj, S.A., Kaarstad, E., Aadnoy, B.S. "Minimizing Friction in Shallow Horizontal Wells", SPE 135812, IADC/SPE Asia Pacific Drilling Technology Conference and Exhibition, Ho Chi Minh, Vietnam, 1-3 November 2010.

Nazari, T., Hareland, G., “Review of Cutting Transport in Directional Well Drilling Systematic Approach”, SPE 132372, Presented at Western Regional Meeting, Anaheim, California, USA, May, 2010.

Niedermayr, M., Pearse, J., and Banks, M., “Case study—Field implementation of Automated Torque and Drag Monitoring for Maari Field Development”,IADC/ SPE 128243 Drilling Conference and Exhibition, New Orleans, USA, February, 2010.

Sheppard, M.C. Wick, C., Burgess, T. “Designing well Paths to Reduce Drag and Torque”, SPE Drilling Engineering, December 1987.

Aadnoy, B.S., Andersen, K. “Design of Oil Wells Using Analytical Friction Models”, Journal of Petroleum Science and Engineering, September 2001.

Aadnoy, B.S., Djurhuus J., “Theory and application of a new generalized model for Torque and Drag”, SPE/IADC 114684, presented at the SPE/IADC Asia Pacific Drilling Tech. Conf. and Exhibition, Jakarta, Indonesia, August 2008.

Aadnoy, B.S., Fazaelizadeh, M., Hareland, G. “A 3-Dimensional Analytica Model for Wellbore Friction”, Journal of Canadian Petroleum Technology, 2010.

Aadnoy, B.S., Kaarstad, E., Theory and Application of Buoyancy in Wells”, SPE/IADC 101795 presented ate the SPE/IADC Asia Pacific Drilling Technology Conference and Exhibition, Bankok, Thailand, November 2006.

8 Appendix

8.1 Derivation of exact equations

8.1.1 Derivation of exact equation for a drop-off bend

By investigating Figure 4.1 we see that the normal force when using polar coordinates is:

$$dN = (F + dF)\, sin\left(\frac{d\varphi}{2}\right) + F \sin\left(\frac{d\varphi}{2}\right) + w\, R \sin\varphi\, d\varphi \tag{83}$$

For small angles (in radians):

$$\sin\left(\frac{\varphi}{2}\right) \approx \left(\frac{\varphi}{2}\right)$$

We get:

$$dN = 2F\left(\frac{d\varphi}{2}\right) + dF\left(\frac{d\varphi}{2}\right) + wR \sin\varphi\, d\varphi$$

And since: $dF\frac{d\varphi}{2} \approx 0$

We then have normal force contribution of:

$$dN = Fd\varphi + wR \sin\varphi\, d\varphi \tag{84}$$

In tangent direction we have:

$$(F + dF)\cos\left(\frac{d\alpha}{2}\right) - F\cos\left(\frac{d\alpha}{2}\right) + \mu|dN| + wRd\varphi\cos\varphi = 0 \tag{85}$$

For small angles (in radians):

$$\cos\left(\frac{d\alpha}{2}\right) \approx 1$$

We then reduce to the incremental friction force which is product of the normal force and friction factor plus projected weight of pipe:

$$dF = \mu|dN| + wRd\varphi\cos\varphi \tag{86}$$

By inserting (84) into (86) we get:

$$dF = (wR\cos\varphi + \mu(F + \mathrm{wRsin}\,\varphi))d\varphi \tag{87}$$

This is an ordinary linear first order differential equation of first degree, and on standard form, it is written like this.

$$\frac{dF}{d\varphi} - \mu F = wR\cos\varphi + \mu\,\mathrm{wRsin}\,\varphi \tag{88}$$

We can solve an equation like (88) by first defining the functions P and Q:

$$P(\varphi) = -\mu \tag{89}$$

$$Q(\varphi) = wR\cos\varphi + \mu\,\mathrm{wRsin}\,\varphi \tag{90}$$

$$I(\varphi) = e^{\int P(\varphi)d\varphi} = e^{\int -\mu d\varphi} = e^{-\mu\varphi} \tag{91}$$

Since we have $F = F_1$ and $\Phi = \Phi_1$

$$F_2 = \frac{F_1 I(\varphi_1)}{I(\varphi_2)} + \frac{1}{I(\varphi_2)}\int_{\varphi_1}^{\varphi_2} I(\varphi)\,Q(\varphi)d\varphi \tag{92}$$

$$F_2 = \frac{F_1 e^{-\mu\varphi_1}}{e^{-\mu\varphi_2}} + \frac{1}{e^{-\mu\varphi_2}}\int_{\varphi_1}^{\varphi_2} e^{-\mu\varphi}(wR\cos\varphi + \mu\,\mathrm{wRsin}\,\varphi)\,d\varphi \tag{93}$$

$$F_2 = F_1 e^{-\mu(\varphi_2-\varphi_1)} + wRe^{\mu\varphi_2}\int_{\varphi_1}^{\varphi_2} e^{-\mu\varphi}(\cos\varphi + \mu\sin\varphi)\,d\varphi \tag{94}$$

$$F_2 = F_1 e^{-\mu(\varphi_2-\varphi_1)} + wRe^{\mu\varphi_2}\left[\frac{e^{-\mu\varphi}}{1+\mu^2}(-\mu\cos\varphi + \sin\varphi - \mu^2\sin\varphi - \mu\cos\varphi)\right]_{\varphi_1}^{\varphi_2}$$

(95)

$$F_2 = F_1 e^{-\mu(\varphi_2-\varphi_1)} + \frac{wRe^{\mu\varphi_2}}{(1+\mu^2)}\left[e^{-\mu\varphi}\left((1-\mu^2)\sin\varphi - 2\mu\cos\varphi\right)\right]_{\varphi_1}^{\varphi_2} \tag{96}$$

Inserting the limits, we end up with the same result as Aadnoy and Andersen (2001) did for hoisting in a drop off bend.

$$\begin{aligned} F_2 = F_1 e^{-\mu(\varphi_2-\varphi_1)} &+ \frac{wR}{(1+\mu^2)}\Big[\Big((1-\mu^2)\sin\varphi_2 - e^{-\mu(\varphi_2-\varphi_1)}\sin\varphi_1\Big) \\ &- 2\mu\Big(\cos\varphi_2 - \cos\varphi_1\, e^{-\mu(\varphi_2-\varphi_1)}\Big)\Big] \end{aligned} \tag{97}$$

8.1.2 Derivation of the equation for a horizontal side bend

By investigating Figure 4.4 we see that the normal force is due to the weight of the pipe and due to tension. If the pipe is resting on the low side, the normal force is then:

$$dN = wRd\alpha \tag{98}$$

The normal force due to tension is:

$$dN = Fd\alpha \tag{99}$$

In reality the pipe will be positioned in between these two extremes, and the resultant normal force will be the vector sum of (98) and (99). The resultant normal force will give the incremental drag by:

$$dF = \mu\sqrt{F^2 + (wR)^2}d\alpha \tag{100}$$

This is an ordinary first order differential equation, and in standard form:

$$\frac{dF}{d\alpha} - \mu\sqrt{F^2 + (wR)^2} = 0 \tag{101}$$

We can separate and integrate:

$$\int \frac{dF}{\sqrt{F^2 + (wR)^2}} = \int \mu \, d\alpha \tag{102}$$

$$ln\left(\frac{F + \sqrt{F^2 + (wR)^2}}{wr}\right) = \mu\alpha + c \tag{103}$$

Inserting $F = F_1$ when $\alpha = \alpha_1$. We then end up with the same result as Aadnoy and Andersen (2001) did. Tension at upper end is then given by:

$$F_2 = \frac{1}{2}\left[\left(F_1 + \sqrt{F_1^2 + (wR)^2}\right)e^{\pm\mu(\alpha_2 - \alpha_1)} - \frac{(wR)^2}{\left(F_1 + \sqrt{F_1^2 + (wR)^2}\right)e^{\pm\mu(\alpha_2 - \alpha_1)}}\right] \tag{104}$$

Where pulling means + and lowering is - .